Unequal-mass, highly-spinning binary black hole mergers in the stable mass transfer formation channel

Aleksandra Olejak, Jakub Klencki, Xiao-Tian Xu, Chen Wang, Krzysztof Belczynski, Jean-Pierre Lasota

A&A, 689, A305 (2024)
https://doi.org/10.1051/0004-6361/202450480

Astronomy & Astrophysics

Unequal-mass highly spinning binary black hole mergers in the stable mass transfer formation channel

Aleksandra Olejak[1,⋆], Jakub Klencki[2], Xiao-Tian Xu[3], Chen Wang[1], Krzysztof Belczynski[4,†], and Jean-Pierre Lasota[4,5]

[1] Max Planck Institut für Astrophysik, Karl-Schwarzschild-Straße 1, 85748 Garching bei München, Germany
[2] European Southern Observatory, Karl-Schwarzschild-Straße 2, 85748 Garching bei München, Germany
[3] Argelander-Institut für Astronomie, Universität Bonn, Auf dem Hügel 71, 53121 Bonn, Germany
[4] Nicolaus Copernicus Astronomical Center of Polish Academy of Sciences, Bartycka 18, 00-716 Warszawa, Poland
[5] Institut d' Astrophysique de Paris, CNRS et Sorbonne Université, UMR 7095, 98bis Bd Arago, 75014 Paris, France

Received 23 April 2024 / Accepted 11 June 2024

ABSTRACT

Context. The growing database of gravitational wave (GW) detections with binary black holes (BHs) merging in the distant Universe contains subtle insights into their formation scenarios.
Aims. We investigated one of the puzzling properties of detected GW sources, namely, the possible (anti)correlation between the mass ratio q of BH-BH binaries and their effective spin $\chi_{\rm eff}$. In particular, unequal-mass systems tend to exhibit higher spins than those with nearly equal-mass BH components.
Methods. We used rapid binary evolution models to demonstrate that the isolated binary evolution followed by efficient tidal spin-up of stripped helium core produces a similar pattern in $\chi_{\rm eff}$ versus q distributions of BH–BH mergers.
Results. In our models, the progenitors of unequal BH-BH systems in the stable mass transfer formation scenario are more likely to efficiently shrink their orbits during the second Roche-lobe overflow than the binaries that evolve into nearly equal-mass component systems. This makes it easier for unequal-mass progenitors to enter the tidal spin-up regime and later merge due to GW emission. Our results are, however, sensitive to some input assumptions, especially the stability of mass transfer and the angular momentum loss during nonconservative mass transfer. We note that mass transfer prescriptions widely adopted in rapid codes favor the formation of BH–BH merger progenitors with unequal masses and moderate separations. We compared our results with detailed stellar model grids and found reasonable agreement after appropriate calibration of the physics models.
Conclusions. We anticipate that future detections of unequal-mass BH–BH mergers could provide valuable constraints on the role of the stable mass transfer formation channel. A significant fraction of BH-BH detections with mass ratio $q \in (0.4{-}0.7)$ would be consistent with having a mass ratio reversal scenario during the first relatively conservative mass transfer and a non-enhanced angular momentum loss during the second highly nonconservative mass transfer phase.

Key words. gravitational waves – binaries: close – stars: black holes – stars: massive

1. Introduction

Recent analysis of detected gravitational wave (GW) sources has reported on the possible negative correlation between mass ratios q (defined as the mass of the less massive object over the more massive object) and the effective spin parameter $\chi_{\rm eff}$[1] among the binary black hole mergers (BH-BH) announced by the LIGO–Virgo–Kagra (LVK) collaboration (Abbott et al. 2023; Callister et al. 2021; Adamcewicz et al. 2023). In particular, unequal-mass BH-BH systems tend to have higher inferred effective spin values than the mergers characterized by equal-mass BH components. If this correlation is real (i.e., not the result of possible degeneracies between individual parameter measurements; see, e.g., Hannam et al. 2013 and Mandel & Smith 2021), it would indicate that a specific mechanism is at work during the formation of at least some current GW sources. Exploring the possibility of such correlations between $\chi_{\rm eff}$ and q by modeling the properties of BH–BH merger populations from different formation channels may help in constraining their relative contributions and put constraints on the uncertain astrophysical processes. McKernan et al. (2022), Vaccaro et al. (2024), and Santini et al. (2023) obtained a similar trend in the $q-\chi_{\rm eff}$ distribution in their models once they combined the synthetic populations of isolated field binaries with a contribution of hierarchical mergers produced in an active galactic nuclei environment.

In this paper, we present an alternative possibility of reproducing the inferred q–$\chi_{\rm eff}$ trend by modeling only isolated binary progenitors of GW sources (Abbott et al. 2023). In particular, we demonstrate that the contribution of BH–BH mergers formed via stable mass transfer (SMT) and common envelope (CE) subchannels may also result in a characteristic pattern in $q-\chi_{\rm eff}$ distribution, similar to the one reported for LVK sources.

The classical isolated binary formation scenario for BH–BH mergers, which has been popular in the literature for several years, includes a CE phase (Belczynski et al. 2016; Eldridge & Stanway 2016; Stevenson et al. 2017; Kruckow et al. 2018; Hainich et al. 2018; Marchant et al. 2019; Spera et al. 2019; Mapelli et al. 2019; Bavera et al. 2020). This scenario consists of an SMT phase during the first

⋆ Corresponding author; aolejak@mpa-garching.mpg.de
† Deceased.

[1] $\chi_{\rm eff} = \frac{m_1\chi_1\cos\theta_1 + m_2\chi_2\cos\theta_2}{m_1+m_2}$, where m_i are BH masses, $\chi_i = cJ_i/Gm_i^2$ are dimensionless spin magnitudes of BHs, θ_i are angles between the individual BH spins and the system's orbital angular momentum, c is the speed of the light in the vacuum, and G is the gravitational constant.

Roche-lobe overflow (RLOF) and a CE (i.e., dynamically unstable mass transfer phase) during the second RLOF. The CE is considered a promising mechanism in binary evolution for bringing an initially wide system close enough to lead to a double compact object merger (Paczynski 1976). However, the significant contribution of the CE scenario has recently been challenged for a few independent reasons. First, several studies have indicated that mass transfer in massive binary systems, such as BH-BH progenitors, is more stable compared to what has been previously found (Ge et al. 2010, 2015, 2020a,b; Pavlovskii et al. 2017; Marchant et al. 2021; Shao & Li 2021). Second, even if unstable mass transfer develops in a system, successful envelope ejection can only happen under very restrictive conditions, making the merger of a donor star and a BH a likely outcome (Kruckow et al. 2016; Klencki et al. 2021; Marchant et al. 2021). As a result, the merger rates predicted for BH-BH systems formed via a CE scenario could be significantly overestimated (Gallegos-Garcia et al. 2021).

In the last few years, the alternative isolated binary BH-BH formation scenario consisting of an SMT phase during the second RLOF (instead of CE) has been gaining popularity in the GW community (see e.g., van den Heuvel et al. 2017; Neijssel et al. 2019; Marchant et al. 2021; Bavera et al. 2021; Olejak et al. 2021; van Son et al. 2022a,b; Olejak & Belczynski 2021; Shao & Li 2021; Broekgaarden et al. 2022; Briel et al. 2023; Dorozsmai & Toonen 2024; Picco et al. 2024). Stable and unstable mass transfer are expected to proceed in specific timescales and differ in the way that masses and orbits evolve. Therefore, the mass transfer stability determines the final fate of the massive binary systems and impacts the distribution of the final masses, orbital parameters, spins, and merger rates of a BH–BH merger population (Olejak et al. 2021; van Son et al. 2022a,b; Bavera et al. 2022; Olejak & Belczynski 2021; Broekgaarden et al. 2022; Dorozsmai & Toonen 2024). When allowing for a relatively conservative mass transfer during the first RLOF, the mass ratio of the binary system may become reversed so that the secondary (initially less massive) star becomes a few times more massive than the primary (initially more massive) star (Olejak & Belczynski 2021; Broekgaarden et al. 2022). If such a significant mass ratio reversal during the first RLOF (to $M_{\rm comp}/M_{\rm don} \gtrsim 3$ at its end) is common, it would favor the formation of unequal-mass BH-BH binaries. We note that some recent analyses of LVK detections have found support for the contribution of such a mass-ratio reversal formation scenario (Broekgaarden et al. 2022; Adamcewicz et al. 2023, 2024) as well as unequal-mass BH–BH mergers (Abbott et al. 2023; Rinaldi et al. 2024; Sadiq et al. 2024).

So far, LVK analysis of the detected BH-BH population is consistent with a distribution dominated by nearly equal-mass component mergers (Abbott et al. 2019). However, some recent works that adopted alternative approaches to infer GW source parameters have found evidence or even a preference for the contribution of unequal-mass ratio BH–BH mergers (Rinaldi et al. 2024; Sadiq et al. 2024). In particular, they have found GW data with BH-BH consistent with a peak in the mass ratio between 0.4 and 0.6, aligning with the distribution derived from our SMT scenario followed by mass ratio reversal. The mass ratio of BH–BH mergers inferred from GW data is, however, uncertain. The general properties extracted for the BH–BH merger population, such as the distribution of the mass ratio, are sensitive to the prior assumptions that are adopted (Farah et al. 2024).

An SMT channel in our models may result in a significant fraction of highly spinning unequal-mass BH–BH mergers (Olejak & Belczynski 2021). This is in contrast to some other recent studies that found that stable mass scenarios are rather unlikely to reproduce detected BH-BH systems with non-negligible $\chi_{\rm eff} > 0$ (Zevin & Bavera 2022) unless they adopt highly super-Eddington accretion on a BH. In this paper, we focus on the properties of BH-BH progenitors in SMT and CE subchannels. We explain why our models, which differ from most of the similar rapid population synthesis codes by their criteria for mass transfer stability, favor the formation of unequal-mass BH–BH mergers with $q \in (0.4{-}0.7)$ and allow for a significant fraction of highly spinning systems. We also test how the properties of produced BH–BH mergers are sensitive to uncertain assumptions on angular momentum loss, BH natal kicks, and mass transfer efficiency.

The paper is organized as follows. In Sect. 2, we describe the method and the relevant physical assumptions adopted in our models. Section 3.1 is devoted to progenitors of BH–BH mergers and understanding the role of the angular momentum loss (Sect. 3.2). Section 3.3 presents the time delay and mass ratio distribution of BH–BH mergers in different tested physical models. Section 3.4 includes evolutionary scenario schema, and Sect. 3.5 addresses the role of natal kicks. In Sect. 4, we discuss other uncertainties and the weak points of modeling binary evolution using rapid population synthesis codes that could affect our results. The discussion includes a brief comparison with BH-star binary grids generated with detailed stellar evolution codes. In Sect. 5, we provide a summary and our conclusions. In the appendix, we address the role of mass transfer instability in tight mass transferring binaries.

2. Method

We used the `StarTrack` population synthesis code (Belczynski et al. 2008, 2020) with a few recent updates (Belczynski 2020; Olejak et al. 2021, 2022) to generate a population of merging BH-BH systems. To evaluate the merger rate density as a function of redshift z, synthetic BH-BH systems were post-processed using the models of star-formation rates and metallicity distribution evolution in the Universe by Madau & Fragos (2017) as described in Dominik et al. (2015) and Belczynski et al. (2020). In the paragraphs below, we address a few subjectively selected physical assumptions most relevant to this study.

Our default model adopts revised mass transfer stability criteria based on the results of Pavlovskii et al. (2017). The authors revisited mass transfer stability for a grid of massive BH-star systems (possible BH-BH progenitors), allowing for high degrees of the RLOF (to the outer Lagrangian point of the donor) and high mass-transfer rates (of a few percent of the dynamical timescale). They found that mass transfer in such types of binaries is significantly more stable than was previously expected. Our revised criteria, as implemented in Olejak et al. (2021), significantly limit parameter space for CE (i.e., unstable mass transfer) development in comparison to what was formerly used (Belczynski et al. 2008). They are characterized by more strictly limited conditions for the mass ratio of the donor to the accertor, which before typically was about two to three (Belczynski et al. 2008) and has now increased to around three to five (Olejak et al. 2021). The new criteria also include extra conditions for donor evolutionary type, radii, and mass to develop unstable mass transfer. The revised criteria have different variants for high ($Z > 0.01$) and low ($Z \leq 0.01$) metallicities. As a result, even binaries with highly unequal masses, such as when the donor is six to seven times more massive than the accretor, may remain stable during the mass transfer phase, depending on

the individual properties of the system. The default version of our criteria, however, takes into account extra parameter space for unstable mass transfer that could develop in tight binaries found, for example, by Pavlovskii et al. (2017), described in Appendix A. The full and detailed description of our mass transfer stability criteria can be found in Sect. 3.1 of Olejak et al. (2021).

For mass transfer onto a nondegenerate accretor, we assumed a fixed accretion efficiency $\beta = 50\%$, where β is a fraction of transferred mass accreted by the companion star, motivated by Vinciguerra et al. (2020), for example. The non-accreted matter is lost from the system with the specific angular momentum of the binary (Podsiadlowski et al. 1992). The possible accretion rate is, however, assumed to be limited by the Eddington rate corresponding to the radius of the accretor[2,3]. In the case of accretion onto a BH component, we adopted the analytic approximations that (King et al. 2001) implemented by Mondal et al. (2020). This approach results in a highly nonconservative mass transfer from the companion to the BH, with the accretion rate onto the BH equal to the Eddington rate (see e.g. King et al. 2023). The non-accreted mass in our default model is lost with the specific angular momentum of the accretor. This assumption, however, has been questioned. For example, Gallegos-Garcia et al. (2023) pointed out that the real angular momentum loss might be much higher once one takes into account such aspects as winds from an accretion disk around the compact objected accretor. Moreover, the presence of a circumbinary disk, which could possibly form after a rapid nonconservative mass transfer phase, could affect the orbital evolution due to interaction between the disk and binary and a possible angular momentum exchange (Pejcha et al. 2016; D'Orazio & Duffell 2021; Zrake et al. 2021; Siwek et al. 2023; Valli et al. 2024). Therefore, in our study, we also tested a model with a significantly higher angular momentum loss for which the material is lost with the specific angular momentum loss of the outer Lagrange point. In our models, we assumed efficient circularization and synchronization due to tides, so during the RLOF, the systems are always on circular orbits. Even if it is at the onset of the RLOF phase, the orbit is still eccentric, and once the mass transfer begins, the system separation is circularized to the periastron (Belczynski et al. 2008).

We adopted the so-called rapid-type SN engine, with the mixing parameter values $f_{\rm mix} = 2.5$ of convection-enhanced supernova engines by Fryer et al. (2022). We assumed that BH formation is accompanied by a natal kick. In our default model, kicks are derived from a Maxwellian velocity distribution with $\sigma = 265\,{\rm km\,s^{-1}}$ (Hobbs et al. 2005). However, their magnitude is decreased by the amount of fallback according to prescriptions by Fryer et al. (2012) and Belczynski et al. (2012). Such a prescription makes massive BHs unlikely to get significant natal kicks. The BH natal kicks are usually expected to be much smaller than the natal kicks of neutron stars (Janka & Kresse 2024). However, the constraints based on the fits to observed systems (Jonker & Nelemans 2004; Repetto et al. 2012; Casares & Jonker 2014; Repetto et al. 2017; Vigna-Gómez et al. 2024) are rather poor so far. Some theoretical studies have indicated that compact object formation might be followed by two independent types of kicks that originate either from asymmetric mass ejection or emission of neutrinos (e.g., Fryer & Kusenko 2006 and Janka & Kresse 2024). Due to the unconstrained nature of BH natal kicks in a few cases, in addition to our default model, we tested an alternative natal kick model with high BH kicks. In that model, the kick velocity is not decreased by fallback. Instead, we reduced the σ of Maxwellian velocity distribution by a factor of two to $\sigma = 133\,{\rm km\,s^{-1}}$. We note that this model results in high BH natal kicks that are much larger than suggested by some recent theoretical predictions (e.g., Janka & Kresse 2024).

Motivated by several massive BH–BH merger detections (with $M_{\rm BH} \geq 50\,M_\odot$), we adopted a high limit for pair-instability supernova (PSN), assuming that stars with their final helium core masses above $M_{\rm He} > 90\,M_\odot$ get disrupted (Belczynski 2020). The high PSN limit is also justified by significant uncertainties in the $^{12}{\rm C}(\alpha,\,\gamma)^{16}{\rm O}$ reaction rate (Farmer et al. 2020; Costa et al. 2021; Woosley & Heger 2021; Farag et al. 2022; Hendriks et al. 2023). We note, however, that the adopted PSN limit does not noticeably affect any of the presented results, such as BH–BH merger rates, mass ratio, or formation scenarios (see, e.g., Olejak et al. 2022). For natal BH spins, we adopted low but nonzero positive values, $\chi \approx 0.05$–0.15 (Belczynski et al. 2020), which were derived under the assumption of efficient angular momentum transport in massive stars (Spruit 2002). We adopted efficient tidal spin-up of stripped helium cores in close BH and stripped helium core systems with orbital periods below 1.1 days (Izzard et al. 2004; Detmers et al. 2008; Kushnir et al. 2016; Hotokezaka & Piran 2017; Zaldarriaga et al. 2018; Belczynski et al. 2020; Bavera et al. 2020).

3. Binary black hole merger progenitors in the stable mass transfer channel

3.1. Stable mass transfer versus common envelope

Evolution through SMT affects the binary orbital separation as well as its components in a different way than the CE phase that later affects the properties of formed BH–BH mergers (for some recent studies see e.g. Olejak et al. 2022; Zevin & Bavera 2022; van Son et al. 2022b; Willcox et al. 2023). Stable mass transfer is expected to produce BH-BH systems that, in general, are wider than CE, as the α prescription widely used by rapid population synthesis for the CE outcome tends to shrink the orbital separation more efficiently than the loss of angular momentum during nonconservative SMT. However, the actual outcome for an individual system depends on its properties at the onset of the SMT or CE phase, in particular the mass ratio between the donor and the accretor as well as the orbital period (see e.g. De Marco et al. 2011; Ge et al. 2022, 2024). Such a dependency produces characteristic fingerprints in the parameter distribution of the BH-BH systems subpopulation that merge within the age of Universe time.

We find that the revised mass transfer stability criteria limiting CE development combined with low (non-enhanced) angular momentum loss during the second SMT phase favor the formation of unequal-mass ratio BH–BH mergers with the characteristic broad peak in a distribution between $q \in 0.4$ and 0.7 (see Sect. 3.2 and Fig. 1)[4]. Moreover, the progenitors

[2] The calculated Eddington rate does not take into account the rapid increase in the total accretor radius expected to happen in case of accretion during the mass transfer on short (thermal and below) timescales (see Lau et al. (2024), Schürmann & Langer (2024)).

[3] That limit mainly affects progenitors of massive BH–BH mergers in the CE subchannel with wide initial orbital separations of $a \gtrsim 800\,R_\odot$.

[4] We note that the emergence of this feature has already been reported by a few other recent studies using `StarTrack` as well as other rapid population synthesis codes when applying similar input assumptions (Olejak et al. 2021, 2022; van Son et al. 2022a,b; Broekgaarden et al. 2022; Dorozsmai & Toonen 2024).

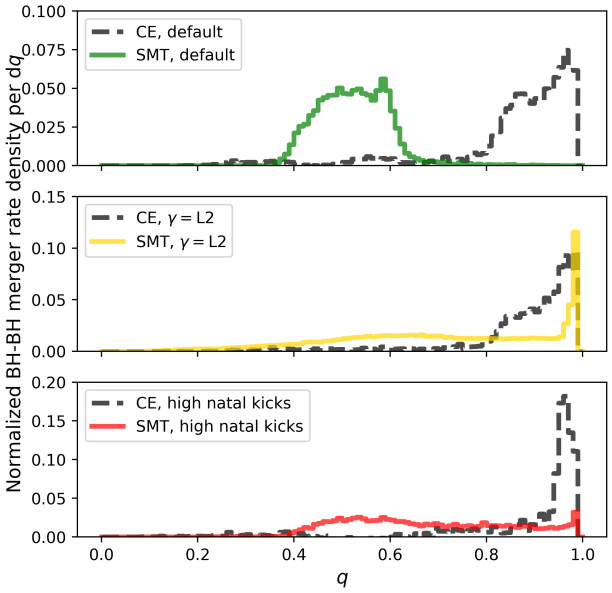

Fig. 1. Mass ratio q distributions of BH–BH mergers (at redshifts $z < 2.0$) formed via an SMT formation scenario (colorful, continuous line) and a CE scenario (black, dashed line) for three tested models. The total sum of the BH-BH merger rate densities normalizes the provided numbers. Results shown are for our default model (upper panel), a model with high angular momentum loss $\gamma = \gamma_{L_2}$ (middle panel), and a model with non-fallback decreased (full) natal kicks (bottom panel; see Sect. 2).

of those unequal BH–BH mergers may experience an efficient tidal spin-up phase at a later evolutionary phase, after which the stripped helium core can produce a rapidly rotating second-born BH (Detmers et al. 2008; Kushnir et al. 2016; Hotokezaka & Piran 2017; Zaldarriaga et al. 2018; Belczynski et al. 2020; Bavera et al. 2020). In our default physical model, within the same set of input assumptions, the CE formation channel is subdominant and tends to produce a nearly equal-mass BH–BH merger with low positive effective spin $\chi_{\rm eff}$ values. The combination of BH–BH mergers formed via the subchannels, with and without CE, results in characteristic $\chi_{\rm eff}$ and q patterns in their distribution in our simulations, shown in Fig. 2.

Our criteria for mass transfer stability limit the development of CE much more than what is typically assumed in the similar types of rapid population synthesis code that are widely used. This explains why other studies did not find an equivalent formation scenario for highly spinning BH–BH mergers via an SMT channel. In particular, in the other codes, highly unequal BH-star systems (the main BH-BH progenitors in our SMT channel) tend to initiate an unstable mass transfer phase during the second RLOF. Therefore, in contrast to our results, studies such as Zevin & Bavera (2022) and Bavera et al. (2022) found that an SMT channel was rather unlikely to reproduce the unequal-mass highly spinning BH–BH mergers. However, with a similar set of physical assumptions (such as mass transfer stability criteria, accretion efficiency, and angular momentum loss), the population of BH–BH mergers in our simulations resembles predictions of other rapid population synthesis codes (see, e.g., Broekgaarden et al. 2022; van Son et al. 2022b in terms of the mass and spin distribution.

In Fig. 3, we present the density grid of BH-star binaries in terms of their orbital periods and mass ratios at the moment of the first BH formation. This grid (in contrast to the similar figures presented in the next Sect. 3.2) also includes the BH-star binaries that evolved through the CE phase. The results are systems that evolved from 100 000 massive stellar binaries with their initial masses in the range $M_1 > 15\,M_\odot$ and $M_2 > 5\,M_\odot$ and with a metallicity of 10% solar ($Z = 0.002$). In the figures, the progenitors of BH–BH mergers in the two subchannels, CE and SMT, are marked with black dots. The figure demonstrates that the progenitors of BH–BH mergers in the two subchannels favor specific separations and mass ratios at the moment of the first BH formation. Progenitors of BH–BH mergers in the CE channel typically have wide separations at the onset of the second RLOF and mass ratios of $M_{\rm star}/M_{M_{\rm BH}} \approx 3$–$4$; these systems can avoid a merger during the CE phase. The BH–BH merger progenitors in SMT are characterized by more extreme mass ratios, $M_{\rm star}/M_{M_{\rm BH}} > 4$, and moderate orbital periods of $P \approx 100$ days. The reason for such specific properties of BH–BH merger progenitors in SMT has been addressed in Sect. 3.2. We note that this is a limited grid of 100 000 massive binaries that we used to demonstrate the preferable mass ratios and separations of BH-BH progenitors for the two subchannels, SMT and CE, in our default model. This model (e.g., due to a relatively conservative mass transfer) produces a significant fraction of unequal-mass BH-star binaries on moderate separations (read more in Sect. 3.2 and discussion in Sect. 4). However, BH–BH mergers can also evolve from different mass ratios and separations. For example, in Fig. 3, the two black dots on the left side corresponding to $M_{\rm star}/M_{\rm BH} \approx 2$ will also later evolve into BH–BH mergers via an SMT subchannel. The stars will initiate the second mass transfer on their core helium-burning phase, losing their envelope in mass transfer and finally evolving into BH-BH binaries with mass ratio $q \approx 0.5$ and a long time delay to the merger of several gigayears.

3.2. The role of the angular momentum loss

The first RLOF in our SMT scenario is relatively conservative. The BH-BH progenitors in this subchannel have an initial separation typically on the order of $\sim 100\,R_\odot$, and they begin mass transfer early after the primary leaves its main sequence. The accretor (main-sequence star) usually gains 50% of the transferred companion mass (see Sect. 2). In contrast, the second RLOF in our models with the accretion rate onto the BH equal to the Eddington rate (King et al. 2023) results in a highly nonconservative mass transfer, and the vast majority of the transferred mass is lost from the system.

The structure of the accretion flow to the BH during the second mass transfer phase is uncertain. The formation of an accretion disk might depend on the BH spin (Sen et al. 2021), which impacts the limit on the accretion rate (Begelman 1979). Even if the disk forms, its geometry and the fraction of mass accreted by a BH is unconstrained (Shakura & Sunyaev 1973; Abramowicz et al. 1988; Tetarenko et al. 2018; Yoshioka et al. 2022; Hu et al. 2022; King et al. 2023; Gallegos-Garcia et al. 2023). The geometry of the accretion determines the angular momentum of the mass lost during nonconservative mass transfer. Accretion efficiency as well as angular momentum of non-accreted material highly affect the orbital evolution of BH-BH system progenitors (MacLeod & Loeb 2020; Willcox et al. 2023; Gallegos-Garcia et al. 2023; van Son et al. 2022b). The amount of specific angular momentum loss during nonconservative mass transfer is often implemented in population synthesis codes as a parameter γ. The below formula gives the response of the orbital separation to binary mass transfer (Tauris & van den Heuvel 2006):

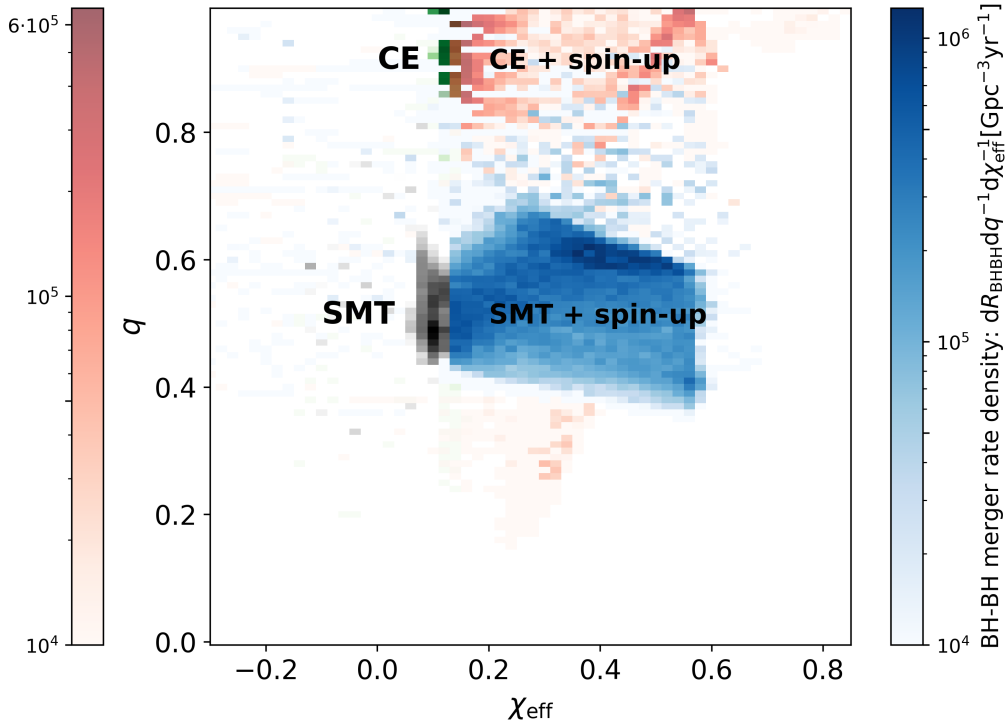

Fig. 2. Two-dimensional $\chi_{\rm eff} - q$ histograms of BH–BH merger rate density $\frac{dR_{\rm BHBH}}{dq d\chi_{\rm eff}}$[Gpc^{-3}yr^{-1}] up to redshifts $z_{\rm mer} < 1.0$ in our default model with the revised mass transfer stability criteria (Pavlovskii et al. 2017; Olejak et al. 2021). The BH–BH mergers have been produced via SMT (black and blue colors) and CE (green and red colors) subchannels. The formation of highly spinning mergers with $\chi_{\rm eff} \gtrapprox 0.15$ was followed by a tidal spin-up phase in close BH-helium core binaries (blue and red colors).

$$\frac{\dot{a}}{a} = -2\frac{\dot{M}_{\rm don}}{M_{\rm don}}\left(1 - \beta\frac{M_{\rm don}}{M_{\rm acc}} - (1-\beta)\left(\gamma + \frac{1}{2}\right)\frac{M_{\rm don}}{M}\right), \quad (1)$$

where β is a fraction of the accreted mass and γ is the dimensionless specific angular momentum of material ejected from the binary.

The commonly adopted assumption is that the ejected material is lost with the specific angular momentum of the accretor, $l_{\rm acc} = \frac{M_{\rm don}}{M_{\rm tot}}\sqrt{GM_{\rm tot}a}$, which implies $\gamma_{\rm acc} = \frac{M_{\rm don}}{M_{\rm acc}}$. That is also the default value in our simulations for a BH accretor. Detailed studies using three-dimensional hydrodynamic models of binary coalescence have indicated that the value of γ depends on the system properties, such as mass ratio (MacLeod & Loeb 2020). In particular, the true amount of angular momentum loss might be significantly higher than $\gamma_{\rm acc}$, varying in the range between $\gamma_{\rm acc}$ and the specific angular momentum of the outer Lagrange point, $l_2 \approx 1.2^2\sqrt{GM_{\rm tot}a}$, corresponding to $\gamma_{\rm L_2} \approx 1.2^2 M_{\rm tot}/(M_{\rm don}M_{\rm acc})$.

We tested how the change in adopted angular momentum loss would impact the properties of BH–BH mergers. In particular, instead of $\gamma = \gamma_{\rm acc}$, we adopted a much higher value $\gamma = \gamma_{\rm L_2}$ accompanying accretion on a BH companion during the second mass transfer phase. We found that our synthetic population of BH–BH mergers is sensitive to our assumption on angular momentum loss. In particular, the tendency of SMT to produce distribution dominated by unequal mass ratio BH–BH mergers is no longer valid once we adopted the high value of $\gamma = \gamma_{\rm L_2}$.

Figure 4 presents the orbital period (in days) versus the mass ratio distribution of BH binaries with a noncompact companion at the moment of the first BH formation. The grids include all BH-star binaries in our simulations that evolved from 100 000 massive binary star systems with their initial masses in the range $M_1 > 15\,M_\odot$ and $M_2 > 5\,M_\odot$. We show the results for the two different metallicities: 1% solar ($Z = 0.0002$, left panels) and 10% solar ($Z = 0.002$, right panels). On top of the density plot, we mark with black dots the systems that later evolved in close BH-BH binaries with their merger time below $t_{\rm GW} < 14$ Gyr. We note that Fig. 4, in contrast to Fig. 3, does not include the systems that at some point of their evolution went (or would go) through a CE phase. We selected only the systems evolving through SMT phases, both for the underlying BH-star binaries (red and yellow density plots) and BH–BH merger progenitors (marked as black dots). The only difference between the top and the bottom panels is the modified angular momentum loss in the case of a BH accretor (the second SMT phase). Therefore, only the systems that later evolved into BH–BH mergers were affected (black dots). The underlying population of BH-star binaries for each metallicity remained the same.

The black dots in the top panels of Fig. 4 show results for our default model with $\gamma = \gamma_{\rm acc}$ during the second nonconservative mass transfer phase with a BH accretor. This model corresponds to relatively low angular momentum loss. In the bottom panels, we demonstrate how BH-BH progenitors are affected once we adopt high values of $\gamma = \gamma_{\rm L_2}$ instead, corresponding to a loss of material with the specific angular momentum loss of the outer Lagrangian point. We find that our default model strongly favors the formation of BH–BH mergers from highly unequal-mass BH-star ($M_{\rm star}/M_{M_{\rm BH}} \geq 3$) systems and with moderate separations of $P \in 10{-}100$ days. The BH-star systems with more equal components or with wide orbital separations evolve into wide BH-BH binaries instead (see more in Sect. 3.3). However, with increased angular momentum loss, progenitors of BH–BH mergers are much more diverse in terms of their mass ratios and period distribution. With high $\gamma = \gamma_{\rm L_2}$, wide BH-star binaries ($P \geq 100$ days) as well tight but more equal-mass systems ($M_{\rm star}/M_{M_{\rm BH}} \leq 2$) can form close BH-BH binaries that merge

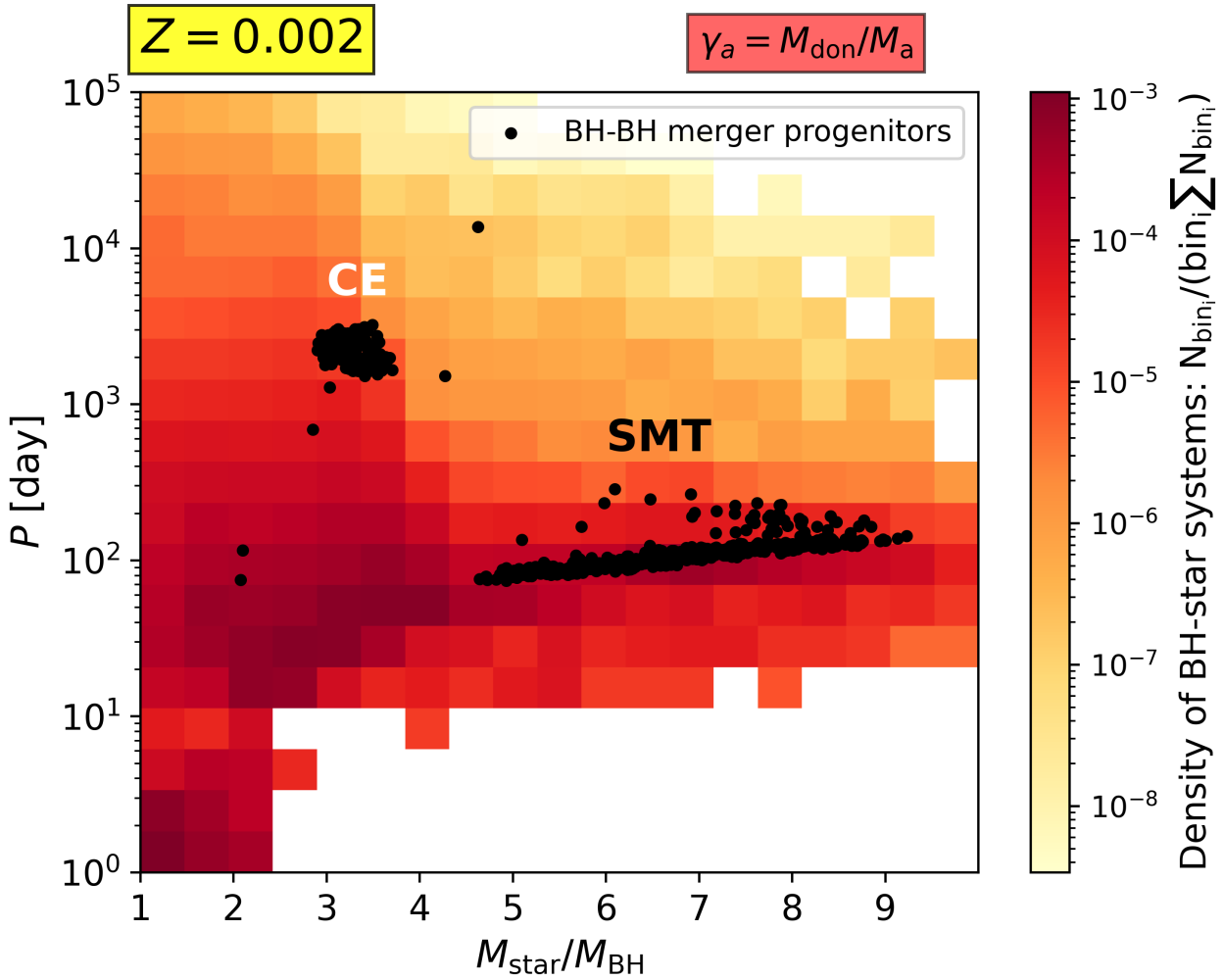

Fig. 3. Orbital period versus mass ratio distribution of BH-star binaries that evolved from initially massive star systems at the moment of the first BH formation. This also includes the systems that evolved through CE. The progenitors of BH–BH mergers via the two formation scenarios, CE and SMT, are marked by the black dots. The presented results are for our default physical model.

in 14 Gyr. Increased angular momentum loss, on the other hand, makes BH-star binaries that are progenitors of BH–BH mergers in the default model merge during the second mass transfer phase. Those systems, with highly unequal masses at the RLOF onset, rapidly shrink their orbits during the mass transfer to the moment when orbital separation no longer fits the donor radius.

The narrow and characteristic parameter space for BH-BH progenitors in our default model is determined by the overlap of several factors:

1. The mass ratio reversal during the first RLOF results in a significant number of BH and massive-star binaries with unequal masses and with moderate orbital periods of $P \in 10-100$ days. The efficient accretion during the first mass transfer phase (typically case A or B) suppresses the formation of BH-star binaries with tight orbits with periods below five to ten days.
2. Only unequal-mass BH-star binaries with a donor several times more massive than a BH might shrink during the SMT of their initial orbit of typically $P \in 10-100$ days to form a close BH-BH system that merges in 14 Gyr.
3. Unequal systems with wide orbital separations $P \geq 10-100$ go through the CE phase, whether they survive or not. Also, unequal tight binaries might experience unstable mass transfer in our default model (see Appendix A). We note that the rapid population synthesis code can underestimate the mass of the donor's core in case it initiates the mass transfer phase during its main sequence (see, e.g., Romero-Shaw et al. 2023). That, besides the assumption on mass transfer efficiency, could lead to more unequal mass ratios and higher separations of BH-star systems than predicted by detailed stellar codes (for more detail, see Sect. 4).

3.3. Time delays

The orbits of BH-BH progenitors are affected in different ways by unstable mass transfer and SMT due to their various timescales, levels of conservation of mass, and accompanying angular momentum loss. Therefore, the final properties of BH–BH merger subpopulations produced via those two subchannels might significantly differ. Because of the still limited understanding of these processes, simplified models that rely on various uncertain assumptions are used to predict the final evolutionary outcome for the systems. The various models result in contrasting properties of formed GW sources, even within the same evolutionary scenario. Specific assumptions may leave characteristic fingerprints in the parameter distribution of the formed BH–BH mergers. For example, we find that when adopting low amounts of angular momentum loss during the nonconserva-

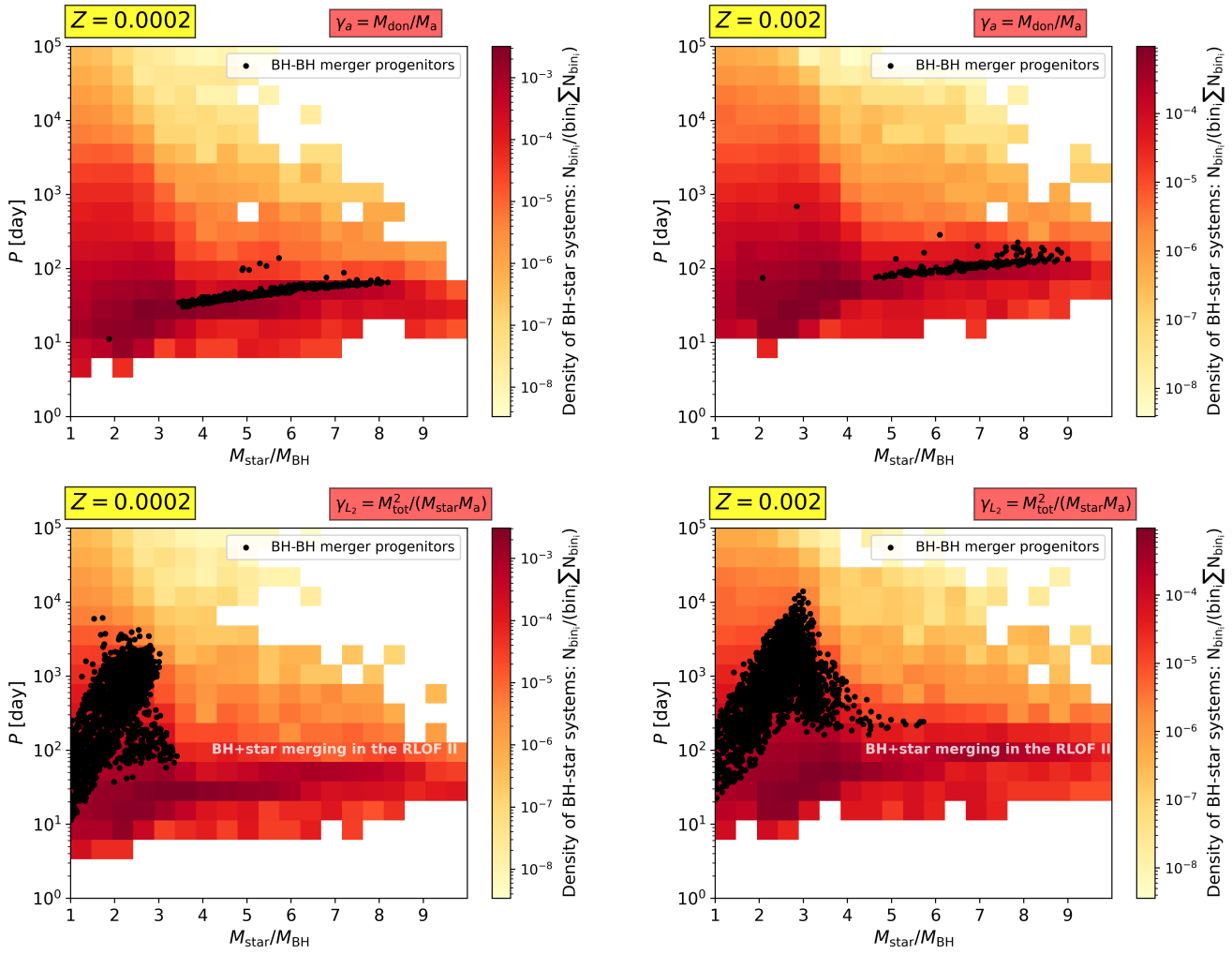

Fig. 4. Orbital period versus mass ratio distribution of BH binaries with a noncompact companion (mainly main-sequence stars). The results shown are only for the SMT subchannel (i.e., they do not include the systems that evolved or would evolve through CE). With the black dots, we mark the progenitors of BH–BH mergers. In the top panel are the systems that become BH–BH merger progenitors once a specific angular momentum loss of the accretor is adopted. In the bottom panels, the black dots mark the systems that would become BH-BH progenitors under assumptions of high specific angular momentum loss, corresponding to the outer Lagrangian point. The left panels are for systems with $Z = 1\%\ Z_\odot$; right panels are for those with $Z = 10\%\ Z_\odot$. The results are for 100 000 generated binary systems with their initial masses in the range $M_1 > 15\ M_\odot$ and $M_2 > 5\ M_\odot$.

tive mass transfer phase, the SMT subchannel strongly favors the formation of unequal-mass BH–BH mergers (Olejak et al. 2021, 2022). In particular, this approach results in a characteristic broad peak in the mass ratio distribution of BH–BH mergers in the range $q \in (0.4–0.7)$, shown in Fig. 1. We discuss the reasons for the peak emergence (e.g., due to orbital response to mass transfer) in Sect. 3.2.

The preference toward unequal-mass BH–BH mergers in the SMT subchannel is well illustrated by the distribution of the BH-BH systems' time delays as a function of their mass ratios in Fig. 5. The red dashed line in the panels separates close BH-BH binaries that merge within 14 Gyr (below) from wide BH-BH systems with time delays above 14 Gyr (above). The upper-left panel of the figure shows the results for our default model with low angular momentum loss, $\gamma = \gamma_{\rm acc}$. The subpopulation of BH-BH systems with short time delays, $t_{\rm del} < 14$ Gyr, consists mainly of the systems with mass ratios in the range of $q \in 0.4–0.7$. Importantly, the same model produces numerous BH-BH systems with nearly equal masses $q \approx 1.0$. However, their orbits are much too wide to merge within the time of the Universe's age. The typical time delays of the equal-mass BH-BH systems vary in the range of $t_{\rm del} \in 10^6–10^{11}$ Gyr.

The relative fraction of equal to unequal-mass BH-BH systems that merge within 14 Gyr is increased when adopting different prescriptions for the natal kicks (see the top-right panel of Fig. 5). When applying high non-fallback decreased BH natal kicks, we significantly decreased the total number of formed BH-BH systems. However, high kicks allow for relatively more systems with comparable component masses to merge in a short time due to their eccentric orbits. The time delay of the BH-BH system merger is $t_{\rm del} \sim (1 - e^2)^{7/2}$ (Peters 1964) (see more in Sect. 3.5, which is devoted to the impact of natal kicks and core collapse physics).

The bottom-left panel of Fig. 5 demonstrates that BH–BH merger mass ratio distribution in our models is highly sensitive to the adopted assumption on the specific angular momentum loss. In this model, the non-accreted material during the second RLOF is lost from the system with the specific angular momentum of the outer Lagrangian point. Increased angular

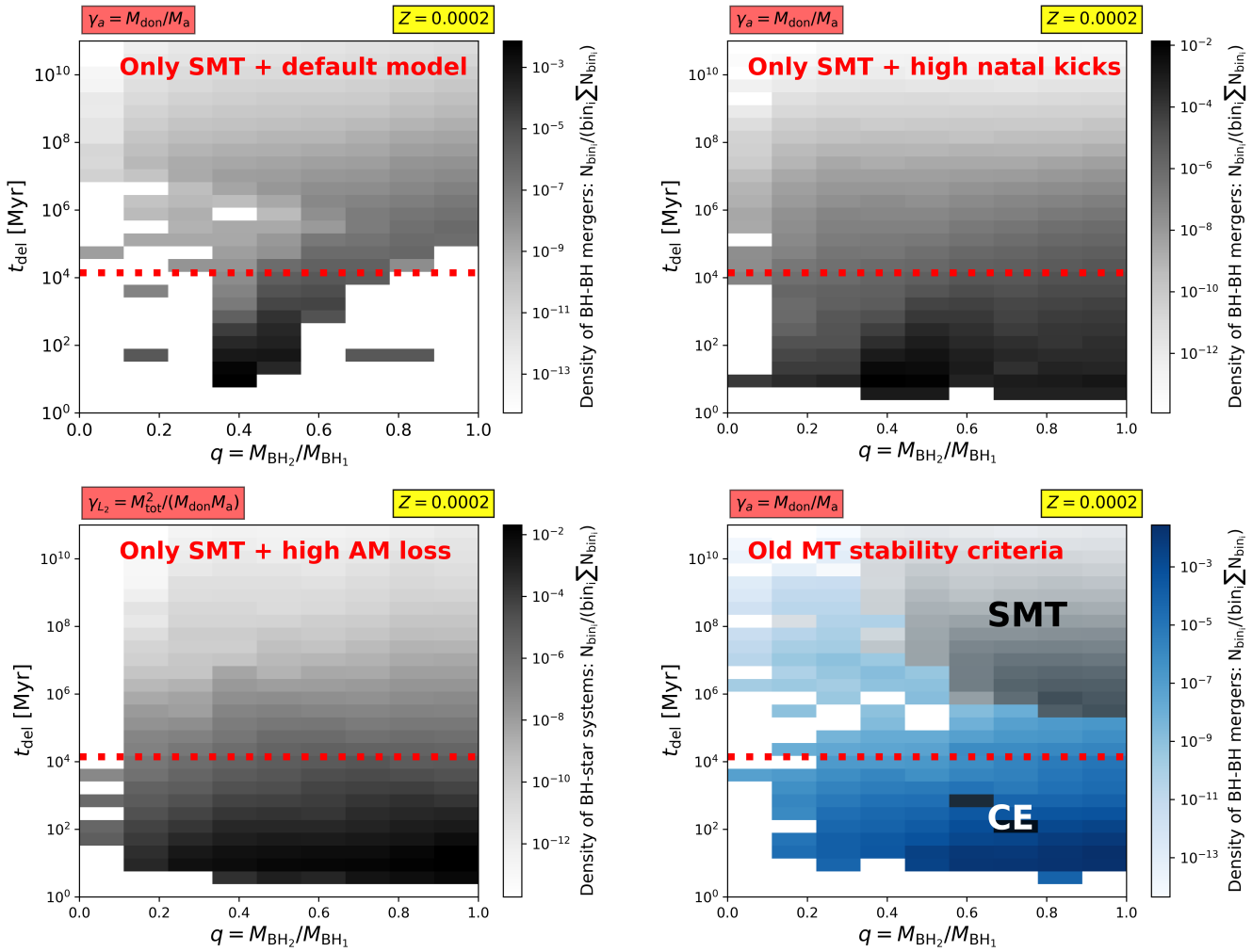

Fig. 5. Time delay (t_{del} [Myr]) versus mass ratio distribution of BH-BH systems in four tested models. The red dashed line corresponds to 14 Gyr. Top-left panel: BH–BH mergers formed via an SMT subchannel in our default model with revised mass transfer stability criteria. This model includes fallback, decreased natal kicks, and low angular momentum loss during nonconservative mass transfer. Top-right panel: BH-BH binaries formed via the SMT subchannel in the model with revised mass transfer stability criteria and low angular momentum loss but non-fallback decreased natal kicks. Bottom-left panel: BH-BH systems formed via the SMT subchannel in the model with revised mass transfer stability criteria and fallback-decreased natal kicks (as in our default model) but high angular momentum loss during nonconservative mass transfer ($\gamma = \gamma_{L_2}$). Bottom-right panel: BH–BH mergers formed by both the CE with $\alpha = 1.0$ (dominant) and the SMT (subdominant) subchannels in the model with old criteria for mass transfer stability.

momentum loss leads to more efficient orbital contraction during the highly nonconservative mass transfer on a BH accretor compared to our default model. Therefore, the progenitors of the equal-mass component BH-BH systems, which in our default model with low $\gamma = \gamma_{acc}$ tend to finish their evolution with wide orbits (time delays orders of magnitudes above the age of the Universe), can then merge in the time of 14 Gyr. As the highly unequal-mass BH-star systems merge during the ongoing mass transfer phase accompanied by high angular momentum loss, in this model, equal-mass component systems are common among BH–BH mergers.

Finally, in the bottom-right panel of Fig. 5, we show the results for the model in which BH–BH mergers, in contrast to our default model, are formed mainly via the CE subchannel (Olejak et al. 2021). This model is much looser in terms of CE development than our default model with the revised mass transfer stability criteria. The BH-BH systems in this model are characterized by rather short time delays, typically below a few gigayears. The distribution is dominated by equal-mass BH–BH mergers. Progenitors in the CE channel, contrary to the SMT scenario, do not experience such a significant mass-ratio reversal during the first RLOF. The initial zero-age main sequence separation of the BH–BH merger progenitors in the CE subchannel is usually one to two orders of magnitude larger than the SMT progenitors, so the first mass transfer is usually initiated at the later part of evolution, once the donor already has a well-defined core-envelope boundary.

Our results indicate that the distribution of the GW sources dominated by equal-mass BH–BH mergers is consistent with both the SMT formation scenarios accompanied by efficient angular momentum loss and the parametrized CE prescription with $\alpha = 1.0$. The inference of GW detections implying a high fraction of unequal-mass BH–BH mergers with their mass ratio $q \in (0.4–0.7)$ could indicate the contribution of an SMT scenario with non-enhanced angular momentum loss. The mass ratio distribution of BH–BH mergers in the CE subchannel, however, can also be affected by core-collapse physics or mass transfer efficiency (see, e.g., Olejak et al. 2022).

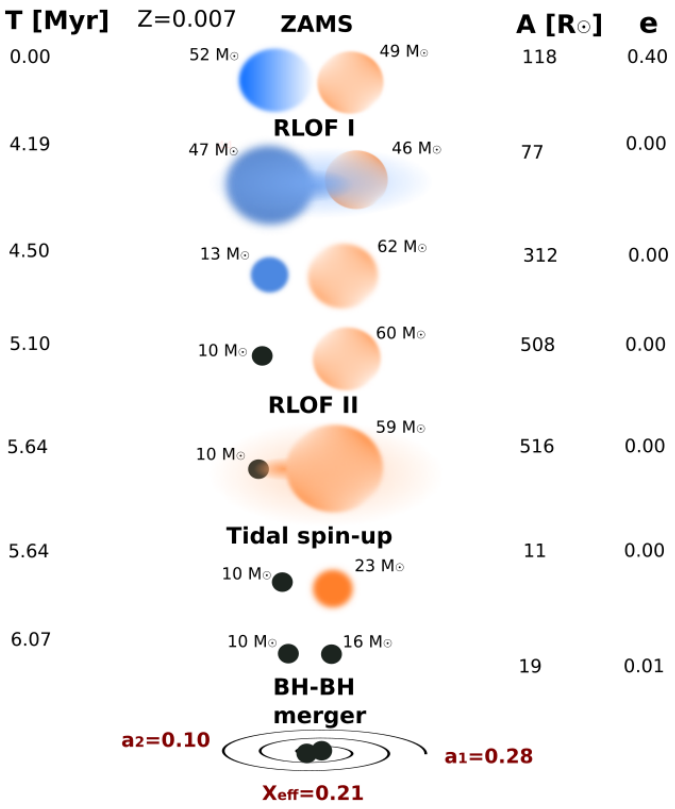

Fig. 6. Typical SMT scenario for the formation of a BH–BH merger with unequal component masses and a high positive effective spin $\chi_{\rm eff} > 0.1$.

3.4. Evolutionary scenario

In this subsection, we present and describe the typical evolutionary scenario for the formation of highly spinning unequal-mass BH–BH mergers via the SMT subchannel in our default model. Figure 6 shows the main stages of the evolution of a binary system.

In contrast to the classic CE scenario (see evolutionary diagrams in, e.g., Belczynski et al. 2016; Olejak & Belczynski 2021), BH–BH merger progenitors in our SMT subchannel typically start their evolution on relatively tight orbits, with an initial separation of several dozen to hundreds of solar radii. This makes the binaries go through the first RLOF phase, while the donor is usually shortly after the main sequence, in the early phase of rapid expansion. The important point of this evolutionary scenario is the mass ratio reversal after the first SMT phase. The companion star (which is initially less massive) gains a large fraction of material transferred from the donor, significantly increasing its mass. The donor loses most of its initial mass and is stripped of its hydrogen envelope, causing only a helium core to remain.

At the moment of the first BH formation, the mass ratio of the binary components is highly unequal (the donor is typically three to seven times more massive than its BH companion), and it has a moderate orbit of $P \in 10{-}100$ days (see Fig. 4). Our BH-BH progenitors then go through the second SMT phase. The donor is usually an early-type radiative envelope giant rapidly expanding after leaving its main sequence. The unequal mass ratio at the onset of the second RLOF allows the systems to effectively shrink their orbits in a highly nonconservative mass transfer onto a BH accretor. The separation and mass ratio systems at the RLOF onset may be so tuned to the loss of angular momentum that the donor is stripped of its hydrogen envelope, while the mass transfer still leads to orbital contraction, producing a very tight BH-helium core binary. We note that systems with such unequal mass ratios but with wider orbits initiate an unstable mass transfer phase within our revised mass transfer stability criteria. If after the second RLOF the orbital period of the BH-helium core binary is below $P_{\rm orb} \lessapprox 1$ day, it then enters the regime of efficient tidal spin-up of the core by a BH. Such an evolutionary scenario (already suggested and described by Olejak & Belczynski 2021 and Broekgaarden et al. 2022) leads to the production of the BH-BH binary in which the second-born high-spinning BH is also the more massive one.

3.5. The role of natal kicks

The mechanism of the natal kicks accompanying compact object formation is uncertain. In the case of BHs especially, the available constraints are very weak. It is expected that the formation of BHs could be followed by partial or even full fallback of matter on the proto-neutron star (Fryer et al. 2012). The magnitudes of natal kicks are usually expected to be significantly lower for BHs than for neutron stars Janka & Kresse (2024). In rapid population synthesis codes, such as `StarTrack`, this relation is approximated by decreasing the possible magnitude of the kick inversely proportional to the amount of fallback onto the newborn compact object (Fryer et al. 2012; Belczynski et al. 2012). Then, progenitors of massive BHs with their pre-supernova (SN) cores above the mass threshold finish their evolution in a "direct collapse," accompanied only by anisotropic emission of neutrinos. The final fate of the star might, however, depend on the details of its final pre-SN structure, which are not included in rapid population synthesis modeling (Sukhbold & Woosley 2014; Patton & Sukhbold 2020; Laplace et al. 2021; Schneider et al. 2021; Fryer et al. 2022; Janka & Kresse 2024). In this subsection, we test how the properties of our synthetic BH–BH merger population are affected by various prescriptions for the final BH masses and the natal kicks they get.

In Fig. 7, we present two-dimensional effective spins $\chi_{\rm eff}$ versus mass ratio q histograms of BH–BH merger rate densities up to redshifts $z < 1.0$. The histograms are only for BH–BH mergers formed via the SMT subchannel and for the two different BH natal kick models. In the left panel, we show the results for our default model with fallback-decreased natal kicks. In the right panel, we present results for the alternative approach with the high BH natal kicks (full, independent of the BH progenitor mass; see Sect. 2). This approach was motivated by a lack of robust observational constraints and a rather poor theoretical understanding of the core collapse and the mechanism of BH natal kicks. So far, high BH natal kicks cannot be ruled out, and they could have interesting and important consequences for the $\chi_{\rm eff}$ distribution of merging BH-BH systems. In particular, they significantly increase the fraction of negative effective spin BH–BH mergers and the contribution of equal-mass events in our SMT channel. We note, however, that this model should be considered as an upper limit on the misaligned BH–BH mergers with $\chi_{\rm eff}$, and some recent studies have suggested much lower BH kicks (see e.g. Janka & Kresse 2024).

High BH natal kicks lead to more frequent disruption of the BH-BH system and a decrease in the total number of formed BH–BH mergers. However, if the BH-BH systems remain bounded, they possibly end evolution on highly eccentric orbits ($e > 0.5$). High eccentricities, on the other hand, significantly

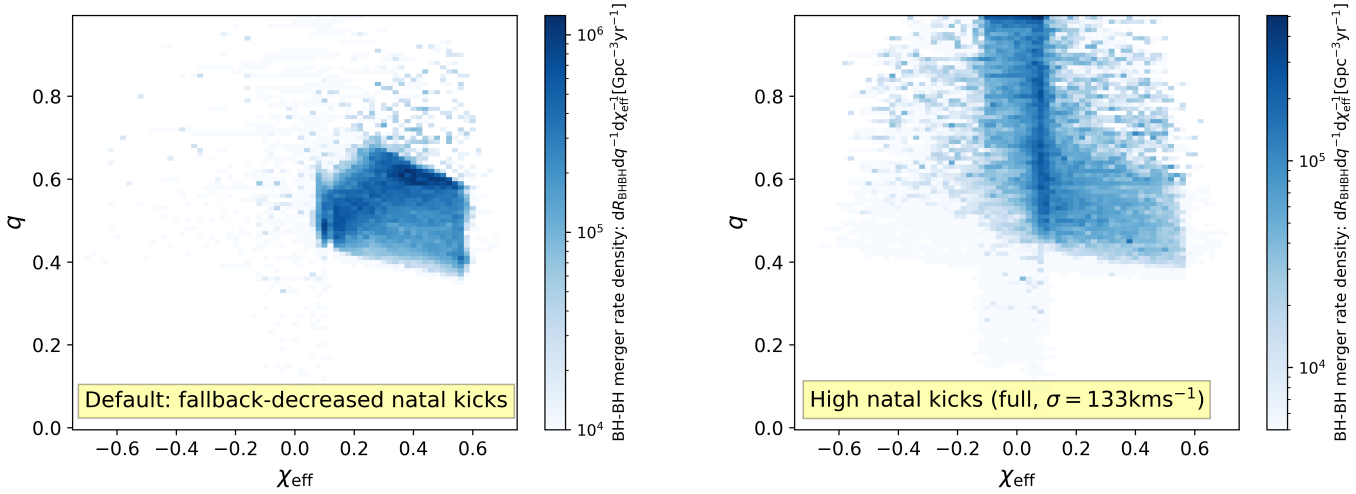

Fig. 7. Two-dimensional χ_{eff} − mass ratio q histograms of the BH–BH merger rates density $\frac{\mathrm{dR_{BHBH}}}{\mathrm{dqd}\chi_{\mathrm{eff}}}$ [$\mathrm{Gpc}^{-3}\,\mathrm{yr}^{-1}$] at redshift $z < 1.0$. This figure only shows the systems formed via the SMT subchannel (CE subchannel not included). We present the results for two natal kick variants. In the left panel is a model with fallback-decreased natal kicks (default), and in the right panel is a model with non-fallback decreased magnitudes (full kick).

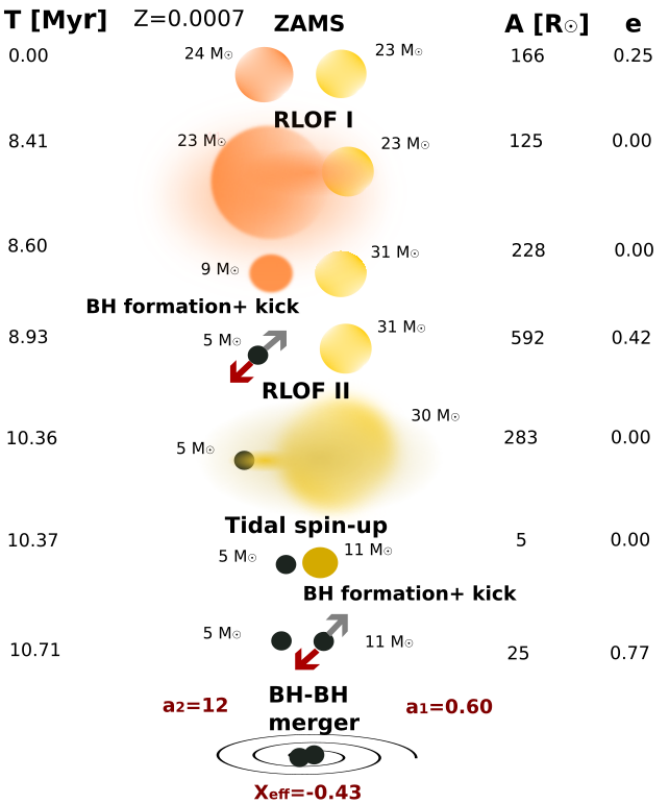

Fig. 8. Stable mass transfer formation scenario of a BH–BH merger with unequal component masses and a high negative effective spin $\chi_{\mathrm{eff}} \approx -0.4$ in the model with full (non-fallback decreased) natal kick magnitudes. This model results in a higher fraction of negative $\chi_{\mathrm{eff}} < 0$ (see right panel of Fig. 7).

decrease expected inspiral time as $T_{\mathrm{ins}} \sim (1-e^2)^{7/2}$ (Peters 1964), allowing eccentric BH-BH systems on wide orbits to merge in a much shorter time (below 14 Gyr). High kicks also increase the fraction of BH–BH mergers with negative effective spins $\chi_{\mathrm{eff}} < 0.0$. Figure 8 presents an evolutionary diagram for the progenitor system of a BH–BH merger that ends its evolution with a very high negative effective spin value of $\chi_{\mathrm{eff}} \approx -0.4$. The formation scenario is similar to the one for the BH–BH merger with a highly positive effective spin presented in Fig. 6. However, in this case, after the efficient tidal spin-up of the helium core by the primary BH, the second-born BH obtains a high natal kick. This causes significant individual BH spin misalignment with the system's orbital momentum axes. The high eccentricity of the wide-formed BH-BH system ($e \approx 0.8$) allows it to merge in the Hubble time.

4. Discussion

4.1. Comparison with detailed stellar model grid

In this section, we present a brief comparison of the grid of the BH-star binaries generated with our `StarTrack` models with a grid obtained using a detailed stellar evolution code. For this second grid, we adopted the BH-MS binaries predicted by Xu et al. (in prep.), which are derived from a dense grid of detailed binary evolution models by Wang et al. (2020). This model grid was computed using the MESA code (version 8845 Paxton et al. 2011, 2013, 2015) with the metallicity of the Small Magellanic Cloud, $Z \approx 0.002 \approx 10\%\,Z_{\odot}$. In the adopted detailed models, critically rotating stars cannot accrete material, which results in near-zero mass transfer efficiencies for all Case B mass transfer. For case A mass transfer, the accretion efficiency is up to about 60%. The star was assumed to end its evolution as a BH once a core helium-depleted star had its helium core mass above $6.6\,\mathrm{M}_{\odot}$, and the yielded compact object was assumed to be a BH (Sukhbold et al. 2018). The final BH mass was computed by ejecting 20% of the mass of the helium envelope and then losing 20% of the mass of the remaining object due to the release of gravitational binding energy (Kruckow et al. 2018). The detailed grids do not include natal kicks for newborn BHs.

There are a few important differences between the input assumptions in our default `StarTrack` model and the detailed model grid. The major ones are the following:

1. A high efficiency of mass transfer on a nondegenerate accretor. In contrast to the detailed models, our default model allows for a much higher fraction ($\beta = 50\%$) of the mass to be accreted during the first RLOF. Donors in our SMT channel are usually early-type giants at the beginning or in the middle of their

expansion, and for that type of binaries, mass transfer in our simulations is expected to be rather efficient[5].
2. Natal kicks and core-collapse physics. Our default model, in contrast to the detailed grids, considers the possible effect of BH natal kicks. This could affect the orbits of the BH-star systems, especially by reducing the number of tight systems with a low-mass BH. The choice of the core-collapse physics also determines the final BH mass. This impacts the mass ratio distribution of systems.
3. Possible underestimation of the post-RLOF donor cores in the case when the mass transfer was initiated during the main sequence. This is a common feature in rapid population synthesis codes that are based on stellar evolutionary tacks by Hurley et al. (2002). The stellar core is not modeled during the main sequence, and when it initiates mass transfer, its mass is approximated by its fit to the stellar mass at the terminal-age main sequence. The underestimation of the donor's core mass during case A mass transfer might shift our mass ratio distribution toward more unequal and wider binaries. Some recent rapid codes implemented ad hoc methods to minimize this effect (see Romero-Shaw et al. 2023).

All of these differences tend to shift BH-star binaries produced by the default `StarTrack` model toward the more unequal mass ratios and wider orbital separations than the binaries predicted by the detailed grid.

Figure 9 demonstrates that once one adopts similar physical input assumptions in `StarTrack` as the ones in the detailed stellar codes, the grids of BH-star binaries begin to overlap well. The panels of the figure present a comparison between the detailed model grid for the 10% solar metallicity (blue color) and different versions of `StarTrack` grids (red color). The left and right panels correspond to the 1% and 10% solar metallicity `StarTrack` grids, respectively.

The upper panels of Fig. 9 show the results for our default model, which adopts relatively efficient mass accretion on the stellar companion ($\beta = 50\%$) during the first mass transfer phase and the standard model for natal BH kicks (fallback-decreased BH kicks). This set of assumptions allows for a common mass ratio reversal during the first RLOF, which allows for the formation of unequal mass BH-star systems with moderate orbital periods. The mass transfer continues after the donor (initially more massive) is less massive than the companion (initially less massive), and during that phase, the binary orbit widens, suppressing the formation of very close BH-star binaries. The orbital period can be further widened by a BH natal kick.

The two bottom panels of Fig. 9 present results for a model with non-efficient mass transfer ($\beta = 0$) and no BH natal kicks ($\sigma = 0\,\mathrm{km\,s^{-1}}$)[6]. Such an input setup is calibrated to match assumptions adopted for the detailed grid. `StarTrack` with the tuned assumptions produces equal-mass BH-star binaries with short orbital periods of $P \lessapprox 5$ days, in agreement with the results for detailed codes.

The effect of metallicity on the populations of BH-star systems produced by StarTrack is complex. In the case of relatively conservative mass transfer with $\beta = 0.5$ and standard BH natal kicks (upper panels of Fig. 9), the orbital periods of the formed BH-star binaries are systematically wider in high metallicity ($Z = 10\%\,Z_\odot$) than in low metallicity ($Z = 1\%\,Z_\odot$). The separation of those systems is already quite wide due to mass ratio reversal during the first RLOF. In high metallicity, the orbits are additionally widened by strong stellar winds and high BH natal kicks (as in the default model, the kicks tend to be inversely proportional to the BH mass).

The model with non-efficient accretion during the first RLOF ($\beta = 0$) and no natal BH kicks (lower panels of Fig. 9) produces a fraction of BH-star systems with nearly equal BH-star masses and with low orbital periods $P \leq 5$ days in both metallicities. Having the accretion limited to zero allowed some of the systems to avoid mass ratio reversal and remain in close orbits after the first RLOF. The mass ratios of these close BH-star systems are less equal in high metallicity, as the final BH mass is reduced by strong stellar winds. This grid is in good agreement with the detailed grid (which is also for the systems with $Z \approx 10\%$) plotted with blue dots in the same figure.

4.2. Other major uncertainties

We point out that the presented results are subject to several other uncertainties apart from the ones tested and described in the earlier sections. In the following paragraphs, we have selected the most relevant uncertainties that could have the most significant effect on the final distribution of mass ratios and spins of our population of BH–BH mergers.

The adopted efficiency of tidal spin-up of the helium cores by a BH companion, and therefore the fraction of a highly spinning second-born BH, might be treated rather as an upper limit. A few factors not considered in our models may significantly decrease the number of highly spinning BH–BH mergers. First, after the mass transfer, we assumed that the donor is completely stripped of its hydrogen envelope. The star may retain some fraction of the hydrogen layer, which later could affect its radius and the fate of the tight binary system. In particular, some of the stripped stars might experience further expansion at a later evolutionary stage and initiate the next phase of (stable or unstable) mass transfer (see Laplace et al. 2020 and Klencki et al. 2022). Second, our adopted simplified approach does not consider a possibly more sophisticated dependency on the metallicity and stellar winds that could weaken tidal interactions by taking away the star's angular momentum as well as by widening the orbit (Detmers et al. 2008).

The increased amount of angular momentum loss during the ongoing mass transfer could also affect its stability. In particular, it could destabilize the mass transfer, leading to higher mass transfer rates and possibly a dynamically unstable mass transfer phase that ends with a successful CE or a merger (Willcox et al. 2023). This effect could also prevent the formation of some BH–BH mergers, especially in the model with increased angular momentum loss $\gamma = \gamma_{L_2}$. Although many BH-star systems merge anyway, due to efficient orbital contraction (and too small of a separation to fit the binary components), that effect might not be fully included in our simulations.

Another important assumption in our simulations is efficient circularization and synchronization due to tides (see Sect. 2) so the systems always enter the RLOF phase on a circular orbit (Hurley et al. 2002; Belczynski et al. 2008). The efficiency of tides is, however, highly uncertain and depends on the stellar

[5] We note that the true mass transfer efficiency is unknown, and both assumptions are justified by the lack of robust constraints. Also, previous studies trying to fit individual observations to determine the accretion fraction are rather divergent in their results (Nelson & Eggleton 2001; Mennickent & Djurašević 2013; de Mink et al. 2007). Some recent studies have even suggested that higher accretion efficiency during Case B than during Case A mass transfer would better reproduce observed systems (Romero-Shaw et al. 2023).

[6] The final BH-star orbits are still mildly affected by the neutrino emission, which in our models is equal to 1% of the pre-core collapse mass of the BH progenitor.

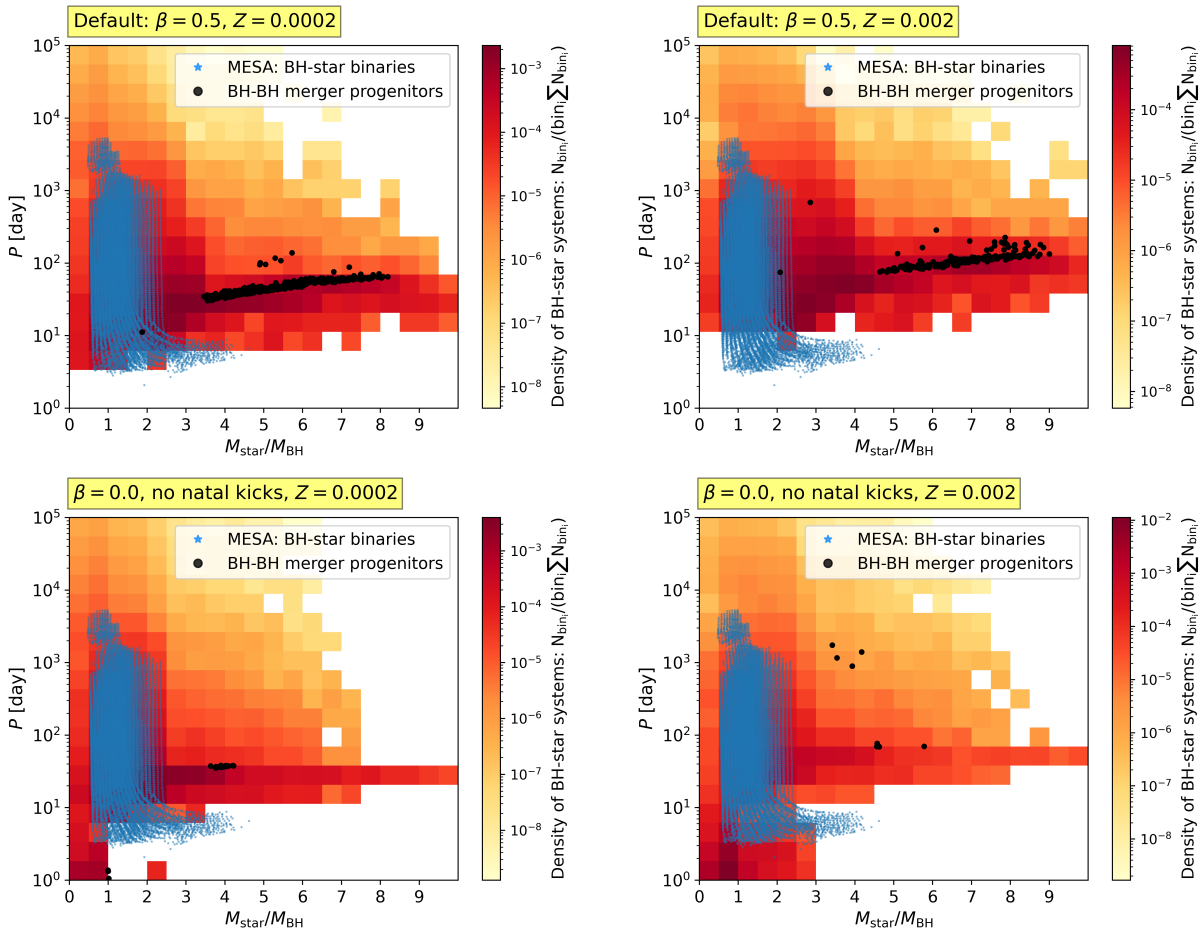

Fig. 9. Density grids of BH-star binaries using our rapid population synthesis code `StarTrack` (red color) and detailed stellar evolution code `MESA` (blue color) from Xu et al. (in prep.). The black points are `StarTrack` BH-star systems that later evolve into BH–BH mergers via the SMT subchannel. The upper panels show the grid for our default `StarTrack` model. The bottom panels are results for the `StarTrack` model with 100% nonconservative mass transfer and no natal kick due to asymmetric mass ejection (except neutrino emission). The left panels are for `StarTrack` models with 1% solar metallicity, and the right panels are for 10% solar metallicity. The detailed grid is for 10% solar metallicity.

structure (Zahn 1977, 1989; Sun et al. 2023; Wu et al. 2024). We note that some observations indicate that binaries could maintain some eccentricity even after the mass transfer phase (Latham 2007; Eldridge 2009; Pauli et al. 2022). In our study, the assumption of efficient circularization may especially affect predictions for the model with high BH natal kicks. While in our default (fallback-decreased) model BHs are born with rather low natal kicks and mild eccentricities, the model with full BH natal kicks results in a significant fraction of highly eccentric systems ($e \gtrsim 0.5$). The uncertainty regarding tidal circularization especially affects the second RLOF phase. After the first BH is formed, the second mass transfer phase could be initiated once the orbit is still eccentric (see formation scenario in Fig. 8). Several studies have tested different approaches to follow the evolution of orbital parameters and mass transfer rates during eccentric RLOF (see e.g. Davis et al. 2013; Dosopoulou & Kalogera 2016a,b; Hamers & Dosopoulou 2019) and found it to be dependent on the system mass ratio. In the case of typical BH–BH merger progenitors in our SMT channel, donors are several times more massive than the accretors at the onset of the second RLOF. For such a mass-ratio regime, eccentricity is expected to decrease or remain constant during the ongoing mass transfer phase (Dosopoulou & Kalogera 2016b; Hamers & Dosopoulou 2019), and the orbital separation is expected to shrink in a manner similar to or more rapidly than in the case of circular RLOF (Hamers & Dosopoulou 2019). Eccentricity at the onset of RLOF could also affect the stability of mass transfer. If the orbital separation shrinks more rapidly in the eccentric case than in the circular one, including eccentricity in our models could possibly lead to more common unstable mass transfer. On the other hand, for radiative-envelope donors, such as our BH–BH merger progenitors in the SMT scenario, it is expected that eventual instabilities would develop with the time delay, possibly allowing the binary orbit to circularize in the meantime due to tides (see e.g. Blagorodnova et al. 2021). Mass transferring binaries with convective-envelope donors could instead initiate CE on eccentric orbits, which would affect the course of the phase and the final outcome (see e.g. Glanz & Perets 2021).

We also point out that our mass transfer stability criteria were approximated by the results for a limited grid of massive binaries and metallicities studied in Pavlovskii et al. (2017). The condition for whether mass transfer in the given system is stable or unstable could be much more complex and sensitive to several other factors, such as eccentricity, or individual properties of the binary, such as chemical composition and the evolutionary stage of the donor (e.g. Ge et al. 2023; Picco et al. 2024). We note that the independent origin of the (anti)correlation between effective spins and mass ratios ($\chi_{\rm eff}$ vs q) of BH–BH mergers formed in isolated binary evolution is the subject of Klencki et al. (in prep.).

5. Conclusions

In this study, we have shown how isolated binary evolution could reproduce the possible anticorrelation between effective spins and mass ratios ($\chi_{\rm eff}$ vs. q) reported for BH–BH mergers (see e.g. Abbott et al. 2023; Callister et al. 2021). We find that our model with revised mass transfer stability criteria limiting CE development and combined with low angular momentum loss during nonconservative mass transfer produces a broad peak of unequal-mass BH–BH mergers with mass ratios in the range $q \in (0.4–0.7)$. When allowing for an efficient tidal spin-up in the close BH-stripped helium core binaries, a significant fraction of those BH-BH systems merge with relatively high effective spins of $\chi_{\rm eff} > 0.2$. The unequal-mass BH–BH mergers are produced by a formation scenario that includes a mass ratio reversal during the first relatively conservative mass transfer and a low angular momentum loss during the second highly nonconservative mass transfer phase. Such a mass ratio reversal scenario as well as a significant contribution of unequal mass ratio BH–BH mergers is consistent with some of the recent analyses of GW detections (Adamcewicz et al. 2023, 2024; Rinaldi et al. 2024; Sadiq et al. 2024). In contrast, the minor fraction of BH–BH mergers produced via a CE phase during the second RLOF tends to have rather equal masses and low spins. Therefore, the combination of the two formation subchannels, that is, the dominant SMT channel and the subdominant CE channel, may constitute a good match for the detected GW systems (Neijssel et al. 2019; Bavera et al. 2021; Olejak et al. 2021; Gallegos-Garcia et al. 2021; van Son et al. 2022b; Dorozsmai & Toonen 2024).

However, the properties of BH–BH mergers are sensitive to uncertain angular momentum loss during the nonconservative mass transfer phase. In particular, the tendency toward the formation of unequal-mass BH–BH mergers in SMT formation scenarios is no longer valid once more efficient angular momentum loss is adopted. When we allowed for high angular momentum loss, the mass ratios of BH–BH mergers became much more diverse. The mass ratio distribution of BH–BH mergers is also affected by core-collapse physics, especially the assumption on BH natal kick magnitudes. High and mass-independent BH natal kicks not only lead to the disruption of many systems but also increase the relative fraction of equal-mass binaries among the population of BH–BH mergers due to high eccentricities. Our aim with this study is to present general trends and their sensitivity to uncertain physical assumptions. We did not try to calibrate our models to best match the detected BH-BH population. We note that the fraction of unequal-mass highly spinning BH–BH mergers in our default model could be overestimated due to the efficient tidal spin-up of the helium core and a few assumptions favoring the production of unequal BH–BH mergers via SMT (see discussion in Sect. 4).

In this study, we have also made a brief comparison of our grid of BH-star binaries with the results of detailed stellar evolution codes. We find that once we adopted equivalent physical input assumptions regarding mass transfer efficiency and BH natal kicks in the rapid population synthesis code `StarTrack`, our grid of BH-star binaries overlapped to a reasonable extent with the one generated using the detailed stellar evolution code `MESA`. Low-mass transfer efficiency, however, reduces the fraction of highly unequal BH-star systems ($M_{\rm star}/M_{\rm BH} \geq 4$), which are the main progenitors of BH–BH mergers in our SMT scenario.

Based on our results, we conclude the following:

1. In contrast to the view widely spread in the GW community, isolated binary evolution does not necessarily favor the formation of BH–BH mergers with equal-mass components. A significant fraction of unequal-mass BH–BH mergers among the future GW detections could indicate the contribution of the isolated binary formation scenario via SMT.
2. The population of BH–BH mergers with the broad peak in mass ratio distribution between $q \in 0.4$ and 0.7 would be consistent with the mass ratio reversal scenario during the first relatively conservative mass transfer and the low angular momentum loss during the second highly nonconservative mass transfer phase. The detection of BH–BH mergers dominated by equal mass-ratio systems is, however, consistent with both SMT channels (e.g., with higher angular momentum loss or high BH natal kicks) and classical CE channels (α formalism), which favor BH formation via direct core collapse.
3. Future observations of binaries of a BH (or evolved star) and massive main-sequence star with a highly unequal mass ratio could imply that the binary experienced an efficient mass transfer phase during the first RLOF. However, observations of tight ($P \leq 5$ days) and equal-mass BH-star systems would challenge the models with a relatively conservative mass transfer phase.

Our predictions will be verified in the near future. The expected significant increase in the number of GW detections with the current and future generation instruments (LIGO Scientific Collaboration 2015; Reitze et al. 2019; The LIGO Scientific Collaboration et al. 2024; Branchesi et al. 2023) combined with progress in their interpretation (Rinaldi et al. 2024; Farah et al. 2024; Fumagalli et al. 2024; Heinzel et al. 2024) and observations of BHs with a noncompact companion in the electromagnetic spectrum with missions such as *Gaia* (Gaia Collaboration 2016, 2024) will provide invaluable lessons on the evolution of massive stars in binary systems and the origin of compact object mergers.

Data availability

Data files underlying this article are available at `https://zenodo.org/records/12530199` or on request. The relevant fragments of the source `StarTrack` code will be shared in response to a request sent to the corresponding author: aolejak@mpa-garching.mpg.de.

Acknowledgements. AO and CW acknowledge funding from the Netherlands Organisation for Scientific Research (NWO), as part of the Vidi research program BinWaves (project number 639.042.728, PI: de Mink). AO acknowledges support from the Foundation for Polish Science (FNP) through the program START 2022 and a scholarship from the Minister of Education and Science (Poland; 2022, 17th edition). AO would like to thank Selma de Mink, Lieke van Son, Daniel Holz, Ilya Mandel, Stephen Justham, Jakob Stegmann, Riccardo Buscicchio, and the reviewer for their useful comments. Sadly, while the work on the article was still in progress, Krzysztof Belczynski passed away. AO would like to thank him for the years of cooperation. JPL lost a friend and collaborator.

References

Abbott, B. P., Abbott, R., Abbott, T. D., et al. 2019, ApJ, 882, L24
Abbott, R., Abbott, T. D., Acernese, F., et al. 2023, Phys. Rev. X, 13
Abramowicz, M. A., Czerny, B., Lasota, J. P., & Szuszkiewicz, E. 1988, ApJ, 332, 646
Adamcewicz, C., Lasky, P. D., & Thrane, E. 2023, ApJ, 958, 13
Adamcewicz, C., Galaudage, S., Lasky, P. D., & Thrane, E. 2024, ApJ, 964, L6
Bavera, S. S., Fragos, T., Qin, Y., et al. 2020, A&A, 635, A97
Bavera, S. S., Fragos, T., Zevin, M., et al. 2021, A&A, 647, A153
Bavera, S. S., Fishbach, M., Zevin, M., Zapartas, E., & Fragos, T. 2022, A&A, 665, A59
Begelman, M. C. 1979, MNRAS, 187, 237
Belczynski, K. 2020, ApJ, 905, L15
Belczynski, K., Kalogera, V., Rasio, F. A., et al. 2008, ApJS, 174, 223
Belczynski, K., Wiktorowicz, G., Fryer, C. L., Holz, D. E., & Kalogera, V. 2012, ApJ, 757, 91

Belczynski, K., Holz, D. E., Bulik, T., & O'Shaughnessy, R. 2016, Nature, 534, 512
Belczynski, K., Klencki, J., Fields, C. E., et al. 2020, A&A, 636, A104
Blagorodnova, N., Klencki, J., Pejcha, O., et al. 2021, A&A, 653, A134
Branchesi, M., Maggiore, M., Alonso, D., et al. 2023, JCAP, 2023, 068
Briel, M. M., Stevance, H. F., & Eldridge, J. J. 2023, MNRAS, 520, 5724
Broekgaarden, F. S., Stevenson, S., & Thrane, E. 2022, ApJ, 938, 45
Callister, T. A., Haster, C.-J., Ng, K. K. Y., Vitale, S., & Farr, W. M. 2021, ApJ, 922, L5
Casares, J., & Jonker, P. G. 2014, Space Sci. Rev., 183, 223
Costa, G., Bressan, A., Mapelli, M., et al. 2021, MNRAS, 501, 4514
Davis, P. J., Siess, L., & Deschamps, R. 2013, A&A, 556, A4
De Marco, O., Passy, J.-C., Moe, M., et al. 2011, MNRAS, 411, 2277
de Mink, S. E., Pols, O. R., & Hilditch, R. W. 2007, A&A, 467, 1181
Detmers, R. G., Langer, N., Podsiadlowski, P., & Izzard, R. G. 2008, A&A, 484, 831
Dominik, M., Berti, E., O'Shaughnessy, R., et al. 2015, ApJ, 806, 263
D'Orazio, D. J., & Duffell, P. C. 2021, ApJ, 914, L21
Dorozsmai, A., & Toonen, S. 2024, MNRAS, 530, 3706
Dosopoulou, F., & Kalogera, V. 2016a, ApJ, 825, 70
Dosopoulou, F., & Kalogera, V. 2016b, ApJ, 825, 71
Eldridge, J. J. 2009, MNRAS, 400, L20
Eldridge, J. J., & Stanway, E. R. 2016, MNRAS, 462, 3302
Farag, E., Renzo, M., Farmer, R., Chidester, M. T., & Timmes, F. X. 2022, ApJ, 937, 112
Farah, A. M., Fishbach, M., & Holz, D. E. 2024, ApJ, 962, 69
Farmer, R., Renzo, M., de Mink, S. E., Fishbach, M., & Justham, S. 2020, ApJ, 902, L36
Fryer, C. L., & Kusenko, A. 2006, ApJS, 163, 335
Fryer, C. L., Belczynski, K., Wiktorowicz, G., et al. 2012, ApJ, 749, 91
Fryer, C. L., Olejak, A., & Belczynski, K. 2022, ApJ, 931, 94
Fumagalli, G., Romero-Shaw, I., Gerosa, D., et al. 2024, arXiv e-prints [arXiv:2405.14945]
Gaia Collaboration (Prusti, T., et al.) 2016, A&A, 595, A1
Gaia Collaboration (Panuzzo, P., et al.) 2024, A&A, 686, L2
Gallegos-Garcia, M., Berry, C. P. L., Marchant, P., & Kalogera, V. 2021, ApJ, 922, 110
Gallegos-Garcia, M., Jacquemin-Ide, J., & Kalogera, V. 2023, ApJ, submitted [arXiv:2308.13146]
Ge, H., Hjellming, M. S., Webbink, R. F., Chen, X., & Han, Z. 2010, ApJ, 717, 724
Ge, H., Webbink, R. F., Chen, X., & Han, Z. 2015, ApJ, 812, 40
Ge, H., Webbink, R. F., Chen, X., & Han, Z. 2020a, ApJ, 899, 132
Ge, H., Webbink, R. F., & Han, Z. 2020b, ApJS, 249, 9
Ge, H., Tout, C. A., Chen, X., et al. 2022, ApJ, 933, 137
Ge, H., Tout, C. A., Chen, X., et al. 2023, ApJ, 945, 7
Ge, H., Tout, C. A., Webbink, R. F., et al. 2024, ApJ, 961, 202
Glanz, H., & Perets, H. B. 2021, MNRAS, 507, 2659
Hainich, R., Oskinova, L. M., Shenar, T., et al. 2018, A&A, 609, A94
Hamers, A. S., & Dosopoulou, F. 2019, ApJ, 872, 119
Hannam, M., Brown, D. A., Fairhurst, S., Fryer, C. L., & Harry, I. W. 2013, ApJ, 766, L14
Heinzel, J., Mould, M., & Vitale, S. 2024, arXiv e-prints [arXiv:2406.16844]
Hendriks, D. D., van Son, L. A. C., Renzo, M., Izzard, R. G., & Farmer, R. 2023, MNRAS, 526, 4130
Hobbs, G., Lorimer, D. R., Lyne, A. G., & Kramer, M. 2005, MNRAS, 360, 974
Hotokezaka, K., & Piran, T. 2017, ApJ, 842, 111
Hu, H., Inayoshi, K., Haiman, Z., et al. 2022, ApJ, 935, 140
Hurley, J. R., Tout, C. A., & Pols, O. R. 2002, MNRAS, 329, 897
Izzard, R. G., Ramirez-Ruiz, E., & Tout, C. A. 2004, MNRAS, 348, 1215
Janka, H. T., & Kresse, D. 2024, arXiv e-prints [arXiv:2401.13817]
Jonker, P. G., & Nelemans, G. 2004, MNRAS, 354, 355
King, A. R., Davies, M. B., Ward, M. J., Fabbiano, G., & Elvis, M. 2001, ApJ, 552, L109
King, A., Lasota, J.-P., & Middleton, M. 2023, New Astron. Rev., 96
Klencki, J., Nelemans, G., Istrate, A. G., & Chruslinska, M. 2021, A&A, 645, A54
Klencki, J., Istrate, A., Nelemans, G., & Pols, O. 2022, A&A, 662, A56
Kruckow, M. U., Tauris, T. M., Langer, N., et al. 2016, A&A, 596, A58
Kruckow, M. U., Tauris, T. M., Langer, N., Kramer, M., & Izzard, R. G. 2018, MNRAS, 481, 1908
Kushnir, D., Zaldarriaga, M., Kollmeier, J. A., & Waldman, R. 2016, MNRAS, 462, 844
Laplace, E., Götberg, Y., de Mink, S. E., Justham, S., & Farmer, R. 2020, A&A, 637, A6
Laplace, E., Justham, S., Renzo, M., et al. 2021, A&A, 656, A58
Latham, D. W. 2007, Highlights Astron., 14, 444
Lau, M. Y. M., Hirai, R., Mandel, I., & Tout, C. A. 2024, ApJ, 966, L7
LIGO Scientific Collaboration (Aasi, J., et al.) 2015, Class. Quant. Grav., 32, 074001
MacLeod, M., & Loeb, A. 2020, ApJ, 893, 106
Madau, P., & Fragos, T. 2017, ApJ, 840, 39
Mandel, I., & Smith, R. J. E. 2021, ApJ, 922, L14
Mapelli, M., Giacobbo, N., Santoliquido, F., & Artale, M. C. 2019, MNRAS, 487, 2
Marchant, P., Renzo, M., Farmer, R., et al. 2019, ApJ, 882, 36
Marchant, P., Pappas, K. M. W., Gallegos-Garcia, M., et al. 2021, A&A, 650, A107
McKernan, B., Ford, K. E. S., Callister, T., et al. 2022, MNRAS, 514, 3886
Mennickent, R. E., & Djurašević, G. 2013, MNRAS, 432, 799
Mondal, S., Belczyński, K., Wiktorowicz, G., Lasota, J.-P., & King, A. R. 2020, MNRAS, 491, 2747
Neijssel, C. J., Vigna-Gómez, A., Stevenson, S., et al. 2019, MNRAS, 490, 3740
Nelson, C. A., & Eggleton, P. P. 2001, ApJ, 552, 664
Olejak, A., & Belczynski, K. 2021, ApJ, 921, L2
Olejak, A., Belczynski, K., & Ivanova, N. 2021, A&A, 651, A100
Olejak, A., Fryer, C. L., Belczynski, K., & Baibhav, V. 2022, MNRAS, 516, 2252
Paczynski, B. 1976, IAU Symp., 73, 75
Patton, R. A., & Sukhbold, T. 2020, MNRAS, 499, 2803
Pauli, D., Oskinova, L. M., Hamann, W. R., et al. 2022, A&A, 659, A9
Pavlovskii, K., Ivanova, N., Belczynski, K., & Van, K. X. 2017, MNRAS, 465, 2092
Paxton, B., Bildsten, L., Dotter, A., et al. 2011, ApJS, 192, 3
Paxton, B., Cantiello, M., Arras, P., et al. 2013, ApJS, 208, 4
Paxton, B., Marchant, P., Schwab, J., et al. 2015, ApJS, 220, 15
Pejcha, O., Metzger, B. D., & Tomida, K. 2016, MNRAS, 455, 4351
Peters, P. C. 1964, Ph.D. Thesis, California Institute of Technology, USA
Picco, A., Marchant, P., Sana, H., & Nelemans, G. 2024, A&A, 681, A31
Podsiadlowski, P., Joss, P. C., & Hsu, J. J. L. 1992, ApJ, 391, 246
Reitze, D., Adhikari, R. X., Ballmer, S., et al. 2019, BAAS, 51, 35
Repetto, S., Davies, M. B., & Sigurdsson, S. 2012, MNRAS, 425, 2799
Repetto, S., Igoshev, A. P., & Nelemans, G. 2017, MNRAS, 467, 298
Rinaldi, S., Del Pozzo, W., Mapelli, M., Lorenzo-Medina, A., & Dent, T. 2024, A&A, 684, A204
Romero-Shaw, I., Hirai, R., Bahramian, A., Willcox, R., & Mandel, I. 2023, MNRAS, 524, 245
Sadiq, J., Dent, T., & Gieles, M. 2024, ApJ, 960, 65
Santini, A., Gerosa, D., Cotesta, R., & Berti, E. 2023, Phys. Rev. D, 108
Schneider, F. R. N., Podsiadlowski, Ph., & Müller, B. 2021, A&A, 645, A5
Schürmann, C., & Langer, N. 2024, A&A, submitted [arXiv:2404.08615]
Sen, K., Xu, X. T., Langer, N., et al. 2021, A&A, 652, A138
Shakura, N. I., & Sunyaev, R. A. 1973, A&A, 24, 337
Shao, Y., & Li, X.-D. 2021, ApJ, 920, 81
Siwek, M., Weinberger, R., & Hernquist, L. 2023, MNRAS, 522, 2707
Spera, M., Mapelli, M., Giacobbo, N., et al. 2019, MNRAS, 485, 889
Spruit, H. C. 2002, A&A, 381, 923
Stevenson, S., Vigna-Gómez, A., Mandel, I., et al. 2017, Nat. Commun., 8, 14906
Sukhbold, T., & Woosley, S. E. 2014, ApJ, 783, 10
Sukhbold, T., Woosley, S. E., & Heger, A. 2018, ApJ, 860, 93
Sun, M., Townsend, R. H. D., & Guo, Z. 2023, ApJ, 945, 43
Tauris, T. M., & van den Heuvel, E. P. J. 2006, Compact Stellar X-ray Sources (Cambridge University Press), 39, 623
Tetarenko, B. E., Lasota, J. P., Heinke, C. O., Dubus, G., & Sivakoff, G. R. 2018, Nature, 554, 69
The LIGO Scientific Collaboration, the Virgo Collaboration, & the KAGRA Collaboration 2024, ApJ, 970, L34
Vaccaro, M. P., Mapelli, M., Périgois, C., et al. 2024, A&A, 685, A51
Valli, R., Tiede, C., Vigna-Gómez, A., et al. 2024, A&A, 688, A128
van den Heuvel, E. P. J., Portegies Zwart, S. F., & de Mink, S. E. 2017, MNRAS, 471, 4256
van Son, L. A. C., de Mink, S. E., Callister, T., et al. 2022a, ApJ, 931, 17
van Son, L. A. C., de Mink, S. E., Renzo, M., et al. 2022b, ApJ, 940, 184
Vigna-Gómez, A., Willcox, R., Tamborra, I., et al. 2024, Phys. Rev. Lett., 132
Vinciguerra, S., Neijssel, C. J., Vigna-Gómez, A., et al. 2020, MNRAS, 498, 4705
Wang, C., Langer, N., Schootemeijer, A., et al. 2020, ApJ, 888, L12
Willcox, R., MacLeod, M., Mandel, I., & Hirai, R. 2023, ApJ, 958, 138
Woosley, S. E., & Heger, A. 2021, ApJ, 912, L31
Wu, S. C., Dewberry, J. W., & Fuller, J. 2024, ApJ, 963, 34
Yoshioka, S., Mineshige, S., Ohsuga, K., Kawashima, T., & Kitaki, T. 2022, PASJ, 74, 1378
Zahn, J. P. 1977, A&A, 57, 383
Zahn, J. P. 1989, A&A, 220, 112
Zaldarriaga, M., Kushnir, D., & Kollmeier, J. A. 2018, MNRAS, 473, 4174
Zevin, M., & Bavera, S. S. 2022, ApJ, 933, 86
Zrake, J., Tiede, C., MacFadyen, A., & Haiman, Z. 2021, ApJ, 909, L13

Appendix A: The role of mass transfer instability in close orbit systems

This section is devoted to the impact of mass transfer instability that might occur in close binaries or orbit systems. It may emerge once the donor star, which is still on its main sequence or early after, responds to the loss of the outer envelope with rapid expansion of deep layers, constantly increasing the relative difference between its radius and its Roche lobe radius. The expansion of internal layers in this type of tight binary happens relatively close to the inner Lagrange point which accelerates the overflow and could lead to instability. The parameter space in terms of the donor masses and radius, for which binary systems experience this type of instability in our models is selected based on the results of Pavlovskii et al. (2017). The detailed description of our revised mass transfer stability criteria together with the mass transfer stability diagram can be found in Sect. 3.1 and Fig. 2 in Olejak et al. (2021).

The emergence of this type of instability in mass-transferring binary star systems impacts the formation of tight BH-star systems. In particular, we find that once we include it in our simulations, we eliminate from our grids close BH-star systems with orbital periods $P < 5$ days. Those binary systems are expected to merge during the unstable mass transfer phase. That, in turn, also limits the number of possible BH–BH merger progenitors. However, the strong preference toward unequal-mass BH-star systems as BH–BH merger progenitors is not affected by including or excluding this type of instability in our models. Those results are demonstrated by the density grid of BH-star binaries and BH-BH progenitors in Fig. A.1. At the top panels, we present BH-star binaries formed in our default model, which includes an extra instability. Black points stand for binaries that later evolve into BH–BH mergers. The bottom panels show the results of the model in which the same systems go through for SMT evolution instead. This model, in contrast to the default one, allows for the formation of equal and moderate mass-ratio BH-star binaries $M_{\rm star}/M_{M_{\rm BH}} \leq 3$ on tight orbits $P < 5 - 10$ days. The presented results are for two metallicities: 1% solar metallicity (on the left) and 10% solar metallicity (on the right). Note that efficient mass transfer on the companion and reversal of mass ratio during the first, SMT phase prevents the formation of close, highly unequal-mass BH-star binaries with $M_{\rm star}/M_{M_{\rm BH}} \geq 5$ no matter if we include an extra instability or not. The impact on BH–BH merger progenitors is visible on the plots. Model without instability slightly increases parameter space for BH-star systems that later evolve into GW sources. However, in both models, BH–BH mergers originate mainly from highly unequal-mass BH-star systems.

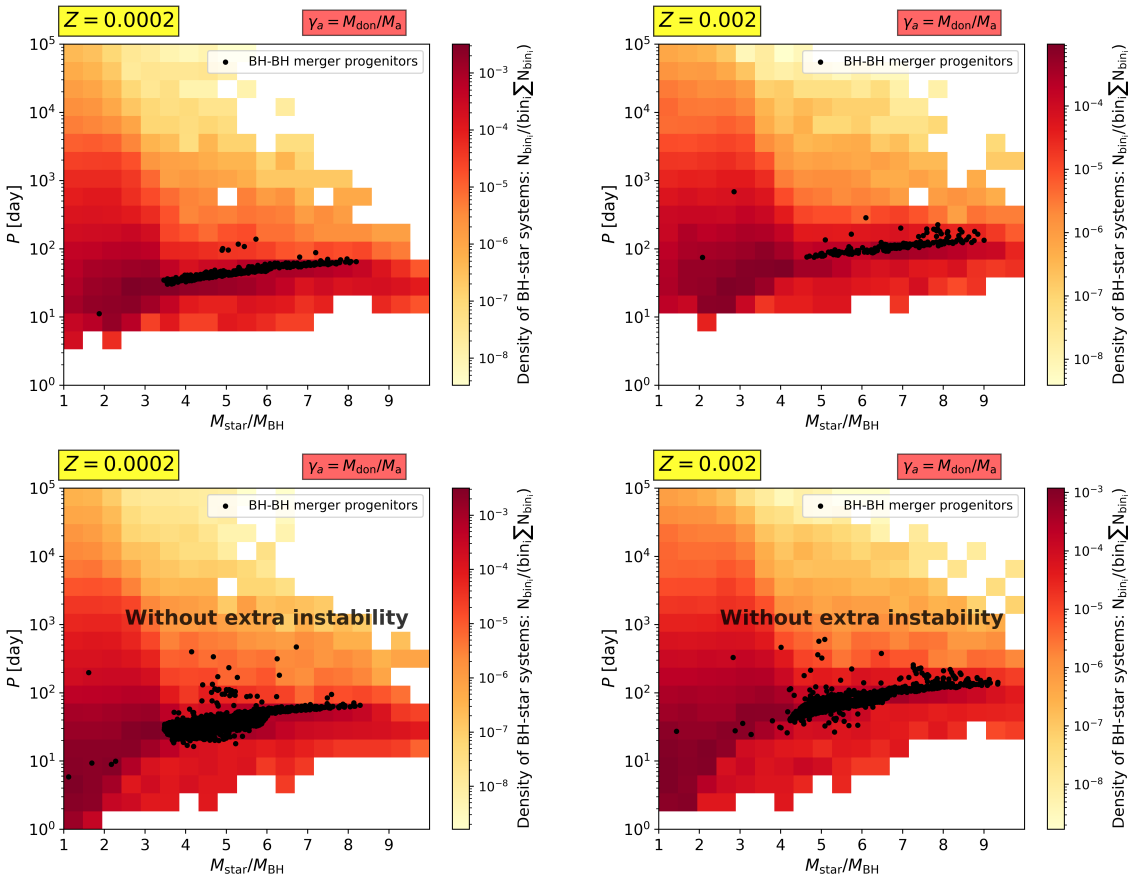

Fig. A.1. Density plot of BH binaries with noncompact companion together with BH-BH progenitors (black points) in a grid of the system mass ratio and orbital period. Results only for the SMT subchannel. Left panels systems with $Z = 1\%\ Z_\odot$, right panels with $Z = 10\%\ Z_\odot$. The top two panels are with BH-star predicted for our default model, which includes the extra instability for tight BH-star binaries. The bottom panels are BH-star binaries formed in the model without the extra instability, which allows tight systems to proceed with SMT instead. This model, in contrast to our default one, produces a fraction of tight BH-star binaries ($P < 5$days) and equal mass ratios. It also allows some of those close BH-star systems to later evolve into BH–BH mergers. Results only for SMT channels, without systems that evolved (or would evolve) through a CE.